Bioactive Materials 49 (2025) 63–84

Contents lists available at ScienceDirect

Bioactive Materials

journal homepage: www.keaipublishing.com/en/journals/bioactive-materials

Zn-DHM nanozymes regulate metabolic and immune homeostasis for early diabetic wound therapy

Shuo Zhang [a,1], Xinyu Zhao [a,1], Wei Zhang [b,1], Xiaolong Wei [b], Xu-Lin Chen [a,*], Xianwen Wang [b,**]

[a] Department of Burns, The First Affiliated Hospital of Anhui Medical University, Hefei, 230032, PR China
[b] School of Biomedical Engineering, Research and Engineering Center of Biomedical Materials, Anhui Medical University, Hefei, 230032, PR China

ARTICLE INFO

Keywords:
Metal-polyphenolic nanozymes
ROS
Metabolic homeostasis
Immune homeostasis
Diabetic wounds

ABSTRACT

Diabetic wounds heal slowly or incompletely because of the microenvironment of hyperglycemia, high levels of reactive oxygen species (ROS), excessive inflammation, metabolic disorders and immune dysregulation, and the therapeutic effect is limited only by disruption of the reactive oxygen species (ROS)-inflammation cascade cycle. Here, a novel metal-polyphenolic nanozyme (Zn-DHM NPs) synthesized by the coordination of Zn^{2+} with dihydromyricetin (DHM) was designed, which not only has a superior ability to scavenge ROS and promote cell proliferation and migration but also functions in the regulation of metabolism and immune homeostasis. *In vitro* and *in vivo* experiments and RNA sequencing analyses revealed that Zn-DHM NPs could increase the levels of intracellular SOD and CAT enzymes to scavenge ROS and maintain the level of the mitochondrial membrane potential to reduce apoptosis. In terms of glucose metabolism, Zn-DHM NPs downregulated excessive levels of intracellular glucose and HK2, inhibited excessive glycolysis and downregulated the AGE-RAGE pathway to restore cellular function. In terms of immune regulation, Zn-DHM NPs not only downregulate M1/M2 levels to promote tissue repair but also maintain Th17/Treg homeostasis, downregulate the IL-17 signaling pathway to reduce inflammation, and upregulate FOXP3 to maintain immune homeostasis, thereby promoting early wound healing in diabetic mice. The development of Zn-DHM NPs provides a new therapeutic target to promote early healing of diabetic wounds.

1. Introduction

Diabetes mellitus is a common chronic metabolic disease in clinical practice [1], and the long-term hyperglycemic state can easily lead to a variety of serious complications, one of which is difficult-to-heal wounds, which affect approximately 25 % of diabetic patients [2], and in severe cases, can lead to amputation, which affects the health and quality of life of patients. Under normal blood glucose conditions, when the skin barrier is damaged, the body initiates a wound healing cascade that stimulates the release of multiple growth factors and promotes neovascularization and the synthesis of extracellular matrices, such as collagen, to regenerate wounds, which often undergo four phases, namely, the hemostatic, inflammatory, proliferative, and remodeling phases [3]. Diabetic wounds, however, have different degrees of cellular dysfunction, cannot complete structural and functional repair of the wound within a specific period of time in each stage, and remain in the chronic inflammatory stage for a long time, making it difficult for them to enter the proliferative stage [4,5]. Therefore, there is an urgent need to understand the mechanism by which diabetic wounds develop into difficult-to-heal wounds and to solve the problem of difficulty in entering the proliferative stage.

In diabetic wounds, prolonged hyperglycemia leads to an increase in advanced glycation end products (AGEs), which, in addition to increasing apoptosis, decreasing cell proliferation, and decreasing the activity of cellular growth factors, can also decrease nitric oxide (NO) levels, leading to delayed tissue repair [6]. Hyperglycemia also reduces the activity of antioxidant enzymes, such as glutathione peroxidase (GSH-Px) and superoxide dismutase (SOD), resulting in reduced free

Peer review under the responsibility of KeAi Communications Co., Ltd.
** Corresponding author.
* Corresponding author.
E-mail addresses: okcxl@126.com (X.-L. Chen), xianwenwang@ahmu.edu.cn (X. Wang).
[1] These authors contributed equally to this work.

https://doi.org/10.1016/j.bioactmat.2025.02.041
Received 30 December 2024; Received in revised form 25 February 2025; Accepted 25 February 2025

radical scavenging and damage [7]. High levels of ROS lead to diminished antioxidant effects in the body, reduced release of cytokines and growth factors, and inhibition of cell migration, collagen fibers and neovascularization [8,9]. Under prolonged hyperglycemia and excessive oxidative stress, macrophages polarize toward the proinflammatory M1 phenotype and secrete inflammatory factors such as IL-6 and TNF-α [10]. Previous studies on the treatment of diabetic wounds have focused on disrupting the ROS-inflammatory cascade cycle, which has achieved some efficacy but not the desired results. Therefore, some scholars have constructed a drug platform that can promote wound healing via multiple mechanisms in accordance with the diabetic wound microenvironment. For example, reducing ROS and hypoxia are synergistically used to promote diabetic wound healing [11], photothermal antibacterial activity and ROS scavenging are synergistically used to promote the healing of diabetic oral ulcers [12], and the activation of inflammatory macrophages is inhibited by inhibiting TLR4-MD2 dimerization and MYD88 phosphorylation [13].

Recent studies have revealed severe immune dysregulation [14] and cellular metabolic disorders [15] in early diabetic wounds. In addition to macrophages [16], naive $CD4^+$ T cells also play an important role in wound healing [17], and under prolonged hyperglycemic conditions, a variety of cytokines lead to an increase in the differentiation of naive $CD4^+$ T cells toward Th17 cells and a decrease in their differentiation toward Tregs, which causes an increase in the release of IL-17 proinflammatory factors, overactivation of the IL-17 signaling channel and amplification of inflammation [18]. FOXP3, the main transcription factor of Tregs, plays an important role in maintaining the balance of the immune system, suppressing inappropriate immune responses and decreasing Treg differentiation, thus leading to immune dysregulation [19]. Although human dermal microvascular endothelial cells (HDMECs) have high value in human skin research, errors in experimental data may occur because of their limited source, specific culture conditions, poor proliferation ability, and easy differentiation or loss of function during culture [20]. To ensure the repeatability and stability of the experimental data, relatively easy-to-culture primary HUVECs were selected as the study cells [21]. In addition, HUVECs are addicted to glycolysis in the early stage of a high-glucose (HG) environment. An increase in the intracellular blood glucose content leads to excessive glycolysis, and excessive intermediates lead to increased bypass metabolism toward polyols, methylglyoxal, etc., causing increased production of byproducts such as AGEs, ROS, and lactate, which leads to endothelial dysfunction and tissue acidification, thus slowing the healing of the wound [22]. Therefore, there is an urgent need to develop a therapeutic strategy that can both prevent oxidative stress and regulate metabolic and immune homeostasis, thereby downregulating the level of inflammation to allow for a smooth transition into the proliferative and remodeling phases for early healing.

Nanozymes are a class of mimetic enzymes that have both the unique properties of nanomaterials and catalytic functions [23]. Since their discovery in 2007, nanozymes have been found to possess enzymatic activities such as SOD, catalase (CAT), peroxidase (POD), etc., and their application in diabetic wounds can scavenge excess ROS and restore the homeostasis of the internal environment [24]; however, the use of some pure metallo-nanoenzymes has been limited due to their toxicity [25,26]. In recent years, metal–polyphenol nanozymes prepared by combining metal nanomaterials with natural antioxidant products have been shown to significantly improve not only their antioxidant and anti-inflammatory capacity, which is easy to prepare, easy to store, and highly biocompatible but also their ability to function as metal ions and compounds originally [27–29]. For example, some scholars have coordinated strontium ions with chlorogenic acid (CGA) to form the metal polyphenol drug (SrC-MPN). The released strontium ions can promote angiogenesis, and CGA can remove ROS, thus effectively improving the microenvironment of diabetic wounds and accelerating healing [30]. Zinc is an essential trace element for human metabolism and growth and plays an important role in various physiological processes as a component of many enzymes [31]. The introduction of exogenous Zn^{2+} can lead to the scavenging of ROS by restoring Cu/Zn SOD activity, and Zn^{2+} can also play an inhibitory role in the activation of signaling pathways, such as the NF-κB and IL-17 pathways, as well as in the production of inflammatory cytokines [32,33]. Zn^{2+} is also involved in the wound healing process, for example, by inducing vascular endothelial growth factor (VEGF) release, promoting angiogenesis, regulating the expression of extracellular proteins such as collagen and keratin, and accelerating epidermal cell division and DNA repair [34]. However, excessive extracellular incorporation of Zn^{2+} can have significant toxic effects on cells by inhibiting manganese uptake and disrupting carbon metabolism. Therefore, a natural polyphenol product needs to be combined with it both to increase its efficacy and to safeguard its biosafety. DHM, a type of flavonoid extracted from vines or Calligonum, has anti-inflammatory, antioxidant, and antimicrobial properties and can control blood lipids and blood glucose via the regulation of cellular metabolism [35]. Functional groups such as the hydroxyl group and the carbonyl group in DHM contain oxygen atoms, which have a strong ability to form coordination bonds with Zn^{2+}, and DHM has a degree of super dissociation and a large π-bond conjugation system, which makes the electron cloud distribution in dihydromyricetin molecules more uniform and enables the formation of stable complexes with Zn^{2+} [36]. Although the antibacterial properties of DHM have been verified [37], early diabetic wounds are generally not accompanied by bacterial infections. Therefore, research on Zn-DHM has focused mainly on antioxidant activity and the regulation of metabolic and immune homeostasis.

Therefore, a metal-polyphenol nanozyme (Zn-DHM NPs) has been reported to scavenge ROS and regulate metabolic and immune homeostasis functions to promote early diabetic wound healing. The main advantages are as follows: 1) The simple synthesis method results in a homogeneous size, stable structure, and good biological properties. *In vitro/in vivo* experiments and RNA sequencing analyses confirmed that 2) in addition to their own superior antioxidant properties and SOD-like enzyme activity, intracellular SOD and CAT activities can also be increased, effectively disrupting the ROS–inflammation cascade cycle. 3) In terms of metabolic regulation, excessive glucose uptake by HUVECs was reduced in a high-glucose environment, excessive levels of intracellular glucose and HK2 were downregulated, and the production of excessive glycolytic products (lactic acid) and glucose metabolism intermediates (AGEs) was inhibited. Therefore, the AGE-RAGE pathway was downregulated, which reduced excessive inflammation, oxidative stress and apoptosis, and cell function was restored. 4) In terms of immune regulation, on the one hand, the M1/M2 level is downregulated to reduce the release of inflammatory factors, and tissue repair is promoted; on the other hand, the homeostasis of Th17/Treg levels is maintained, the differentiation of naive $CD4^+$ T cells into Th17 cells is reduced, and the IL-17 signaling pathway is downregulated, which reduces inflammation and promotes wound remodeling. In addition, the differentiation of naive $CD4^+$ T cells into Tregs is increased, which upregulates the FOXP3 factor to maintain immune homeostasis. Notably, Zn-DHM NPs promoted cell proliferation, migration, angiogenesis, collagen deposition, and epithelialization through the upregulation of DNA replication and repair, thereby facilitating the early healing of wounds in diabetic mice with good biosafety. This work highlighted that Zn-DHM NPs have good potential for the early treatment of diabetic wounds (see Scheme 1).

2. Results and discussion

2.1. Synthesis and characterization of Zn-DHM NPs

In this study, $ZnCl_2$ and DHM were synthesized via self-assembled coordination to form size, uniform and structurally stable metal–polyphenol nanozyme Zn-DHM NPs (Fig. 1A). The color of the $ZnCl_2$ solution fully dissolved by ultrasonication was milky white, and there was no

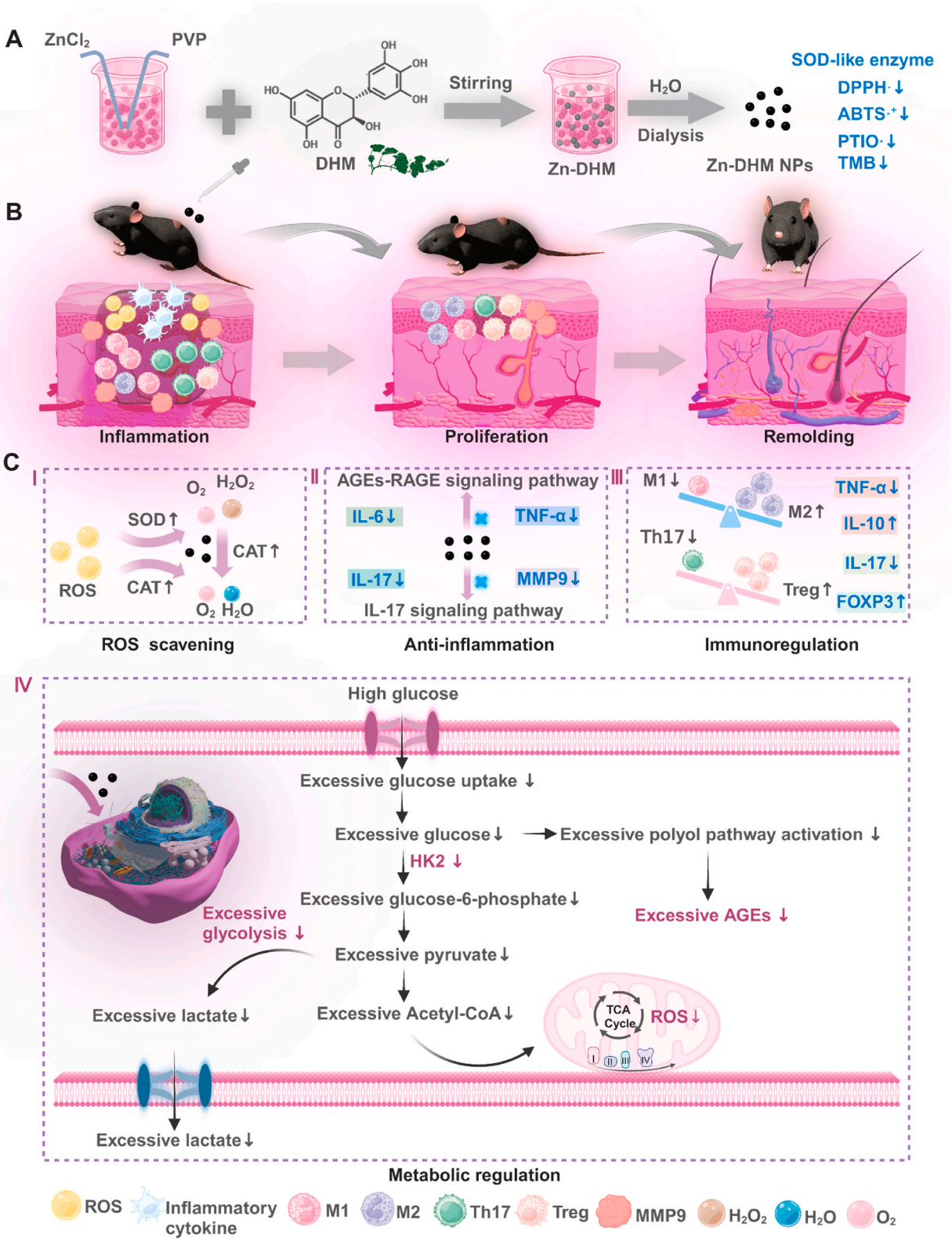

Scheme 1. **(A)** The synthesis process and antioxidant properties of Zn-DHM NPs. **(B)** Diabetic wounds from the inflammation phase to the proliferation and remolding phases. **(C)** The mechanism of promoting early diabetic wound healing: ROS scavenging (I), anti-inflammation (II), immunoregulation (III) and metabolic regulation (IV).

obvious color change when it was added to the polyvinyl pyrrolidone (PVP) solution; however, when the DHM solution was added dropwise, the reaction solution inside the beaker showed a light yellow change, indicating that a chemical reaction between DHM and $ZnCl_2$ occurred, resulting in the formation of a new type of substance, i.e., Zn-DHM NPs. With increasing stirring time, the color of the reaction mixture in the beaker gradually increased from light yellow to golden yellow and brown, indicating that the content of Zn-DHM NPs increased

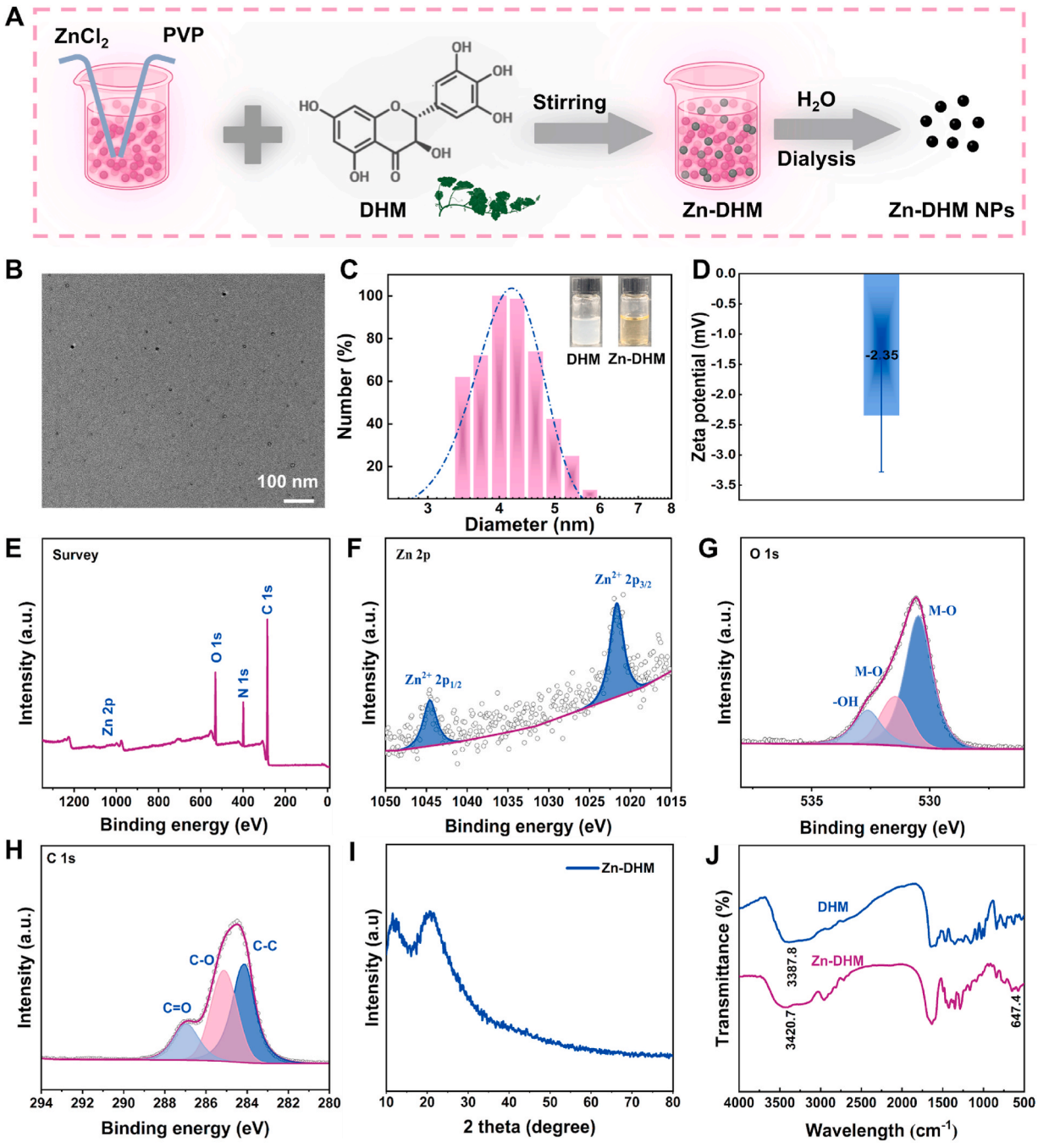

Fig. 1. Synthesis and characterization of Zn-DHM NPs. (**A**) Mechanistic diagram of synthesis. (**B**) TEM images of Zn-DHM NPs. (**C**) DLS of Zn-DHM NPs. (**D**) Zeta potential of the Zn-DHM NPs. (**E-H**) XPS survey spectra. (**I**) XRD pattern of Zn-DHM NPs. (**J**) FTIR spectra of Zn-DHM NPs.

continuously. PVP is a water-soluble polymer compound with excellent surface activity, thickening ability, and adsorption ability. After encapsulation by PVP, the drug solubility and increased stability of the Zn-DHM NPs improved. TEM clearly revealed the microsphere-like structure of the Zn-DHM NPs, which had a homogeneous structure and extremely small size, with a diameter of approximately 5 nm (Fig. 1B), which was in agreement with that measured by DLS (Fig. 1C). When the Zn-DHM NPs were dissolved in pure water, the zeta potential of their surface ranged from −3.34 mV to −1.48 mV (Fig. 1D). After XPS detection, the first results revealed that the Zn-DHM NPs consisted of Zn, C, N, and O, which are Zn 2p at 976.08 eV, O 1 s at 531.08 eV, N 1 s at 399.08 eV, and C 1 s at 285.08 eV, respectively (Fig. 1E). The spectral peaks of the elements were further analyzed, and Zn 2p peaks were found at 1044.48 eV and 1021.58 eV (spectral peaks of Zn^{2+} $2p_{1/2}$ and Zn^{2+} $2p_{3/2}$) (Fig. 1F). The spectral peak of O 1 s at 532.58 eV was M − O (Fig. 1G), and the spectral peaks of C 1 s at 286.98 eV, 286.98 eV, and 286.98 eV were C=O, C-O, and C-C, respectively (Fig. 1H). These results indicate that the valence of the Zn ions in the Zn-DHM NPs is +2, which further verifies the successful coordination of Zn^{2+} with DHM. The XRD results revealed the presence of Zn in the Zn-DHM NPs, which have an amorphous structure (Fig. 1I). A comparison of the FTIR data of DHM with those of Zn-DHM NPs revealed that the Zn-DHM NPs presented broad and strong characteristic hydroxyl stretching vibration peaks at 3300~3500 cm^{-1}. The 4-position carbonyl vibration frequency in the DHM molecule was located at 1639.5 cm^{-1}, and it moved to 1634.7 cm^{-1} when DHM formed a coordination complex with Zn^{2+}, which

indicated that the carbonyl oxygen of DHM is involved in coordination. Owing to the bonding of metal ions, the bonding electron density of the carbonyl group is shifted farther from the geometric center of the bond to the oxygen atom, which reduces the double bonding of the carbonyl group; therefore, the stretching vibration of the carbonyl group shifts the absorption band to a lower frequency. The frequency region of the aryl ring skeleton vibration of C=C is from 1450 cm^{--1} to 1600 cm^{--1}, and the corresponding absorption peaks appear in this region for DHM and Zn-DHM NPs; the displacement wavenumber is not obvious, indicating the existence of a benzene ring structure. The DHM and Zn-DHM NP molecules at the C-O-C bond vibration frequency (1050 $cm^{-}1$~1250 cm^{-1}) were essentially unchanged, suggesting that the C-ring ether bonds did not open. The new absorption peak of the complex at 647.4 cm-1 can be attributed to the stretching vibration and bending vibration absorption of M-O; that is, Zn^{2+} coordinates with DHM to synthesize Zn-DHM NPs via Zn-O bonds (Fig. 1J). The results of inductively coupled plasma emission spectrometry (ICP–OES) revealed that the content of elemental Zn was 10 μg/mg in the Zn-DHM NPs, and the concentration of Zn-DHM NPs used in all the subsequent experiments was related to the Zn content.

2.2. Antioxidant properties and enzyme-like activities of Zn-DHM NPs

High levels of ROS are a typical feature of the diabetic wound microenvironment and can lead to cell dysfunction associated with tissue regeneration, attracting more inflammatory cells to the lesion. Drugs that eliminate excessive ROS can significantly promote the healing of diabetic wounds [38,39]. To determine whether Zn-DHM NPs can have

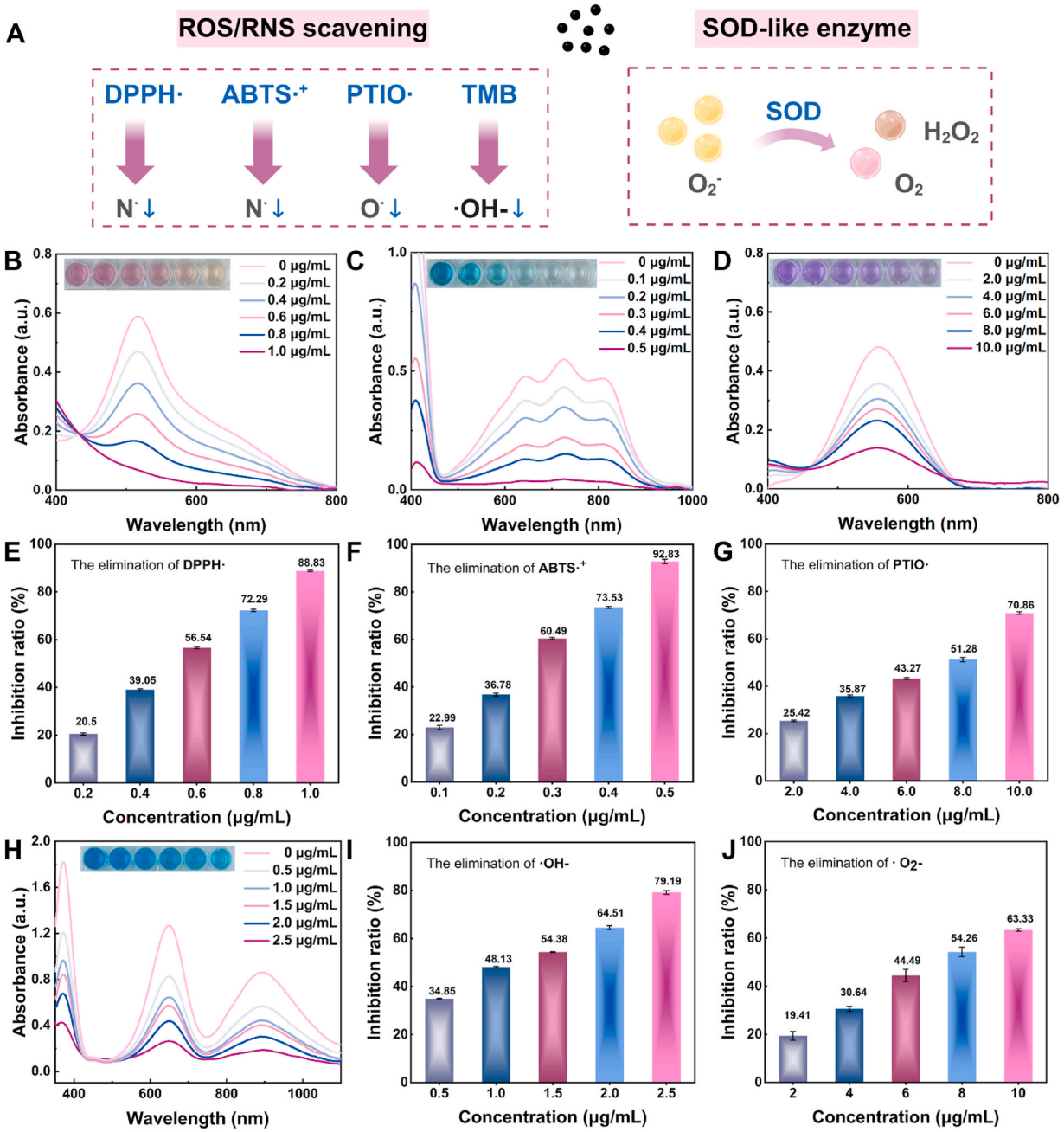

Fig. 2. Antioxidant properties and enzyme-like activities of Zn-DHM NPs. (**A**) Mechanistic diagram of ROS/RNS scavenging and SOD-like activity. (**B, E**) DPPH· scavenging and elimination. (**C, F**) $ABTS^{\cdot+}$ scavenging and elimination. (**D, G**) PTIO· scavenging and elimination. (**H-I**) ·OH- scavenging and elimination. (**J**) SOD-like activity and elimination of $\cdot O_2$-. The error bars represent the means ± SDs (n = 3).

antioxidant capacity, four probes, DPPH·, $ABTS^{\cdot+}$, PTIO· and TMB, were used, and the results revealed that the Zn-DHM NPs have strong ROS/RNS scavenging capacity. A superoxide dismutase (SOD) enzyme kit was used to test enzyme-like activity, and the results revealed that the Zn-DHM NPs possessed SOD enzyme-like properties and were able to catalyze the disproportionation of $\cdot O_2$- into H_2O_2 and O_2 (Fig. 2A).

DPPH· is a stable neutral radical with one unpaired electron, i.e., an odd number of electrons on the N atom, which has a maximum absorption peak at 517 nm, and the solution is dark purple. With increasing Zn-DHM NP concentration, the color of DPPH gradually changed from dark purple to light purple and yellowish within 5 min, and its absorption peak at 517 nm decreased. When the concentration of Zn-DHM NPs was 1 μg/mL, the OD_{517} decreased from 0.60 a.u. to 0.07 a.u. (Fig. 2B), and the scavenging rate almost reached 88.83 % (Fig. 2E), indicating its superior performance in scavenging N· radicals. ABTS can be oxidized by potassium persulfate, and after 12 h of reaction, $ABTS^{\cdot+}$ cationic radicals are generated, with single electrons also present on the N atoms, which has a maximum absorption peak at 734 nm, and the solution is blue–green in color. To further verify the ability of Zn-DHM NPs to scavenge RNS, different concentrations of Zn-DHM NPs were added to the $ABTS^{\cdot+}$ test solution. With increasing concentrations of Zn-DHM NPs, the color of the $ABTS^{\cdot+}$ test solution gradually changed from blue–green to light-green and white within 5 min, and its absorption peak at 734 nm also decreased. When the concentration of Zn-DHM NPs was 0.5 μg/mL, the OD_{734} decreased from 0.55 a.u. to 0.04 a.u. (Fig. 2C), and the scavenging rate almost reached 92.83 % (Fig. 2F), which again verified that its ability to scavenge N· radicals was extremely strong. PTIO·, similar to DPPH·, is also a stable neutral radical, but its single electrons are on the O atom, and it has a maximum absorption peak at 557 nm in a blue–violet solution. With increasing concentrations of Zn-DHM NPs, the color of the PTIO· test solution gradually changed from blue–violet to light–violet within 10 min, and its absorption peak at 557 nm decreased. When the concentration of Zn-DHM NPs was 10.0 μg/mL, the OD_{557} decreased from 0.48 a.u. to 0.14 a.u. (Fig. 2D), with a scavenging rate of almost 70.86 % (Fig. 2G), indicating its superior ability to scavenge O· radicals. TMB reacts with ·OH- to form a dark blue substance with a maximum absorption peak at 650 nm. To determine whether Zn-DHM NPs have the ability to scavenge ·OH-, ferrous sulfate first reacts with H_2O_2 to generate ·OH- via the Fenton reaction, and after the generation of visible bubbles, different concentrations of Zn-DHM NPs are added to the reaction mixture, and finally, the TMB test solution is added. The results revealed that the color of the test solution gradually changed from dark blue to light blue within 5 min with increasing Zn-DHM NP concentration, and its absorption peak at 650 nm decreased. When the concentration of Zn-DHM NPs was 2.5 μg/mL, the OD_{650} decreased from 1.28 a.u. to 0.27 a.u. (Fig. 2H), and the clearance rate was almost 79.19 % (Fig. 2I), indicating the superior performance of the Zn-DHM NPs in scavenging ·OH-.

SOD is an important antioxidant enzyme in organisms that can catalyze the reaction of $\cdot O_2$- to produce H_2O_2 and O_2 [40]. WST-8 reacts with $\cdot O_2$- to produce a formazan dye, which has a maximum absorption peak at 450 nm. To determine whether Zn-DHM NPs have the ability to remove $\cdot O_2$-, first, xanthine oxidase (XO) was used to catalyze the production of $\cdot O_2$-, and different concentrations of Zn-DHM NPs were added to the reaction mixture. Finally, the working solution of WST-8 was added, and the change in absorbance was observed. The results revealed that the absorption peak at 450 nm decreased with increasing concentrations of Zn-DHM NPs, and when the concentration of Zn-DHM NPs was 10 μg/mL, the clearance was almost 63.33 % (Fig. 2J), which indicated that the Zn-DHM NPs had good SOD-like enzyme activity. In addition, the abilities of the $ZnCl_2$, DHM and Zn-DHM subgroups to remove DPPH (Fig. S1) and PTIO (Fig. S2) **were compared**, and the results revealed that the Zn-DHM subgroups were significantly more effective than the $ZnCl_2$ and DHM subgroups.

The above probe and kit results indicated that the Zn-DHM NPs had strong ROS/RNS scavenging ability and SOD-like enzyme properties, which provided a theoretical basis for the subsequent *in vitro* cellular and *in vivo* experiments.

2.3. Zn-DHM NPs promote cell proliferation, migration and tube formation in vitro

Zn^{2+} and DHM have good pro-tissue repair functions [41]. To verify whether the Zn-DHM NPs have the properties of the two ligands, we performed CCK8, Transwell, tube-forming, and scratch experiments. The results revealed that the Zn-DHM NPs promoted the proliferation, migration, and tube formation of HUVECs *in vitro* and promoted the epithelialization of L929 cells, which was superior to the effects of $ZnCl_2$ and DHM (Fig. 3A).

First, the CCK8 assay was conducted to detect HUVEC activity by setting the concentration grouping, and the results showed that when the concentration of Zn-DHM NPs was less than 50 μg/mL, it had a proproliferative effect on HUVECs, and the best effect was achieved at a concentration of 20 μg/mL. When the concentration of Zn-DHM NPs was greater than 50 μg/mL, it had an inhibitory effect on the activity of the cells (Fig. S3). The cell activity assay was performed at a 20 μg/mL mass concentration for 1, 3, and 5 days, and it was found that Zn-DHM NPs not only had a good pro-proliferative effect on HUVECs but also had good biosafety (Fig. S4). The $ZnCl_2$, DHM, and Zn-DHM NP subgroups were established, and the results of the CCK8 activity assay revealed that the Zn-DHM NPs promoted the proliferation of HUVECs better than the $ZnCl_2$ and DHM subgroups did (Fig. S5). Owing to the presence of nutrients such as serum in the bottom chamber of the Transwell system, HUVECs can be induced to migrate from the top chamber to the bottom chamber. The results after adding the same concentration of different materials to the bottom chamber revealed that at 6 h, compared with the control group, the $ZnCl_2$, DHM, and Zn-DHM NP groups promoted HUVEC migration, and the number of Zn-DHM NPs was approximately 337, which was significantly greater than that of the $ZnCl_2$ and DHM groups (Fig. 3B, and E). The results of the tube formation assay and ImageJ vascular analysis revealed that at 6 h, the length of blood vessels formed by Zn-DHM NPs promoted by HUVECs was approximately 190 % of that of the control group, which was significantly greater than that of $ZnCl_2$ and DHM (Fig. 3C, and F). Similarly, a CCK8 assay was used to detect toxicity to L929 cells. The results revealed that the Zn-DHM NPs promoted the proliferation of L929 cells at a concentration of 20 μg/mL (Fig. S6). Therefore, this concentration was selected for subsequent experiments. The effects of Zn-DHM NPs and ligands on the migration and repair of L929 cells were detected via scratch experiments, and the results revealed that Zn-DHM NPs promoted the healing rate of scratches by 49.19 % and 83.32 % at 12 h and 24 h, respectively, which was greater than that of the $ZnCl_2$ and DHM groups (Fig. 3D, and G).

The above experimental results showed that Zn-DHM NPs, with the properties of Zn^{2+} and DHM, could significantly promote cell proliferation, migration, tube formation and epithelialization and were superior to the $ZnCl_2$ and DHM group, which implies that Zn-DHM NPs play an important role in the wound healing process.

2.4. Zn-DHM NPs attenuate HG-induced oxidative stress and protect mitochondrial function

Vascular injury and neovascular dysfunction are among the mechanisms by which diabetic wounds develop into difficult-to-heal wounds [42], which mainly involve vascular endothelial cell dysfunction caused by high glucose [43]. To simulate the microenvironment of high-glucose injury *in vivo*, the present study established a HG-injured HUVEC model and confirmed that Zn-DHM NPs could increase the activities of intracellular SOD and CAT to accelerate the scavenging of intracellular ROS, increase the level of the mitochondrial membrane potential (MMP), and reduce the degree of apoptosis, as demonstrated by ROS staining, JC-1 staining, AM/PI staining, and SOD and CAT detection kits (Fig. 4A).

ROS staining and flow cytometry assays revealed that HG treatment

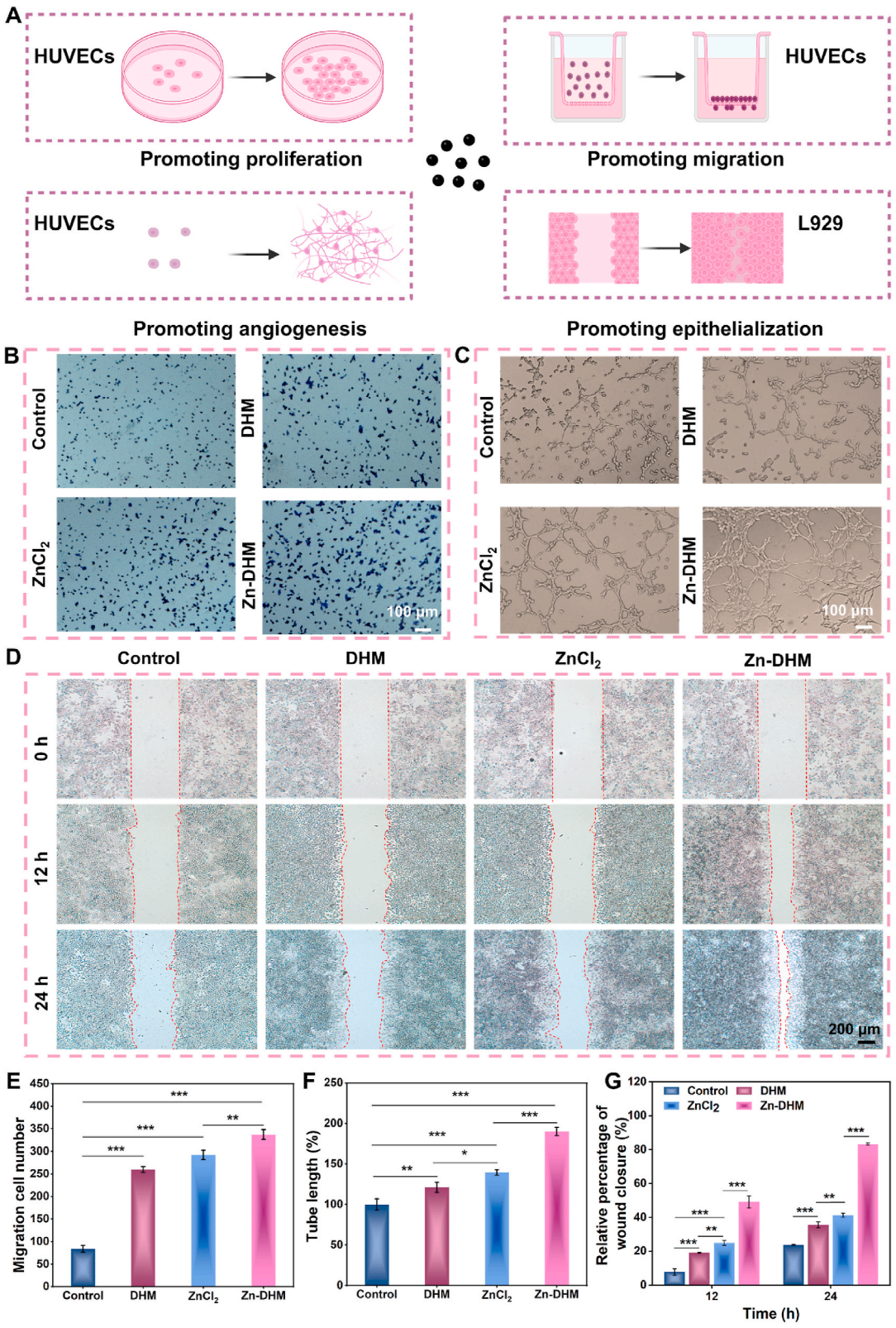

Fig. 3. Zn-DHM NPs promote cell proliferation, migration and tube formation *in vitro*. (**A**) Mechanistic diagram of the function test. (**B, E**) Transwell analysis of HUVECs and statistical analysis via ImageJ. (**C, F**) Tube formation of HUVECs and statistical analysis by ImageJ. (**D, G**) Scratching experiments with L929 cells and statistical analysis with ImageJ. The error bars represent the means ± SDs (n = 3, ***P < 0.001, **P < 0.01, and *P < 0.05).

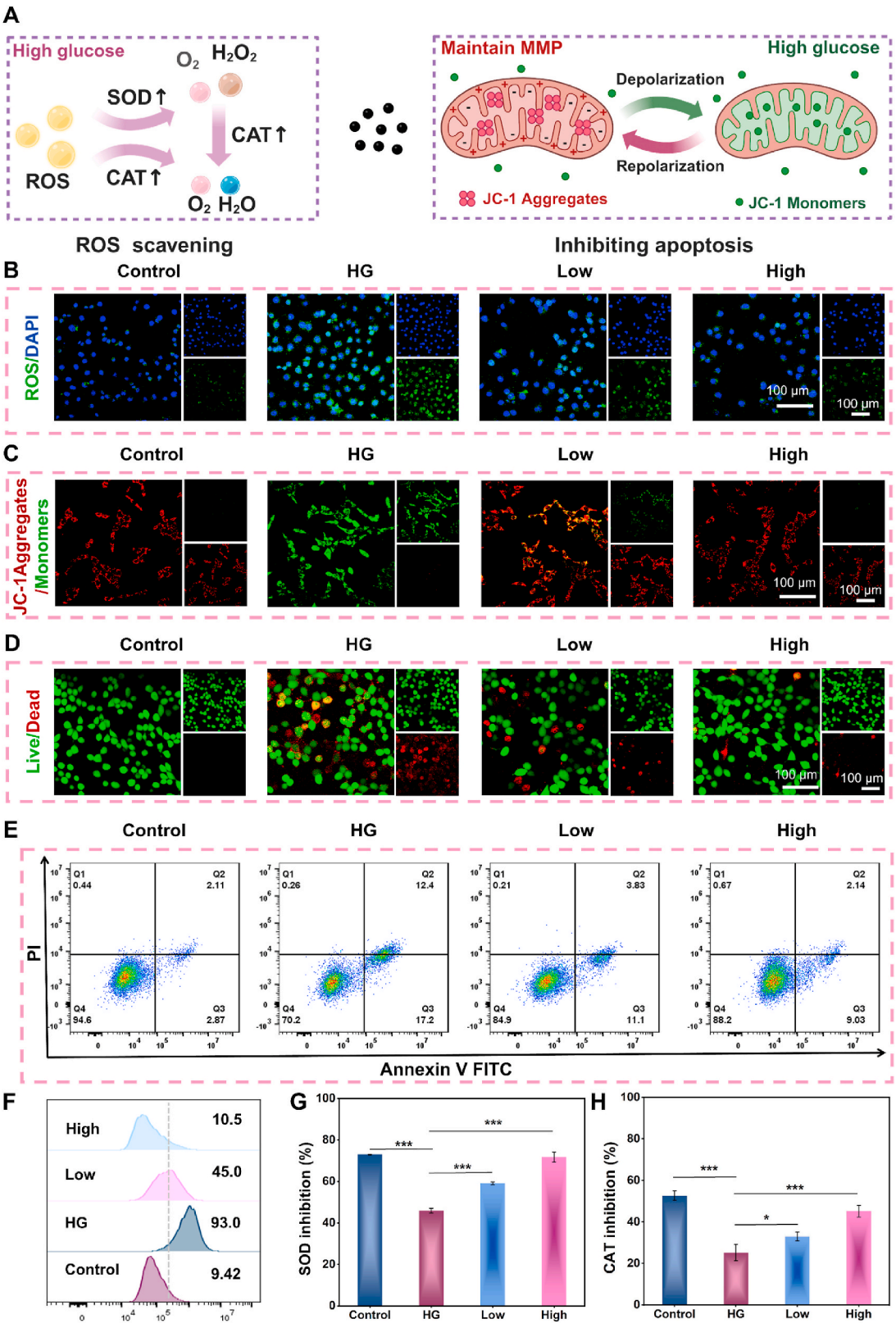

Fig. 4. Zn-DHM NPs attenuate HG-induced oxidative stress and protect mitochondrial function. (**A**) Mechanistic diagram of antioxidative stress and the inhibition of apoptosis. (**B**) ROS fluorescence staining. (**C**) JC-1 fluorescence staining. (**D**) AM/PI fluorescence staining. (**E**) Annexin V/PI flow cytometry assay. (**F**) ROS flow assay. (**G**) SOD activity in cells. (**H**) CAT activity in cells. Low = HG + Zn-DHM (10 μg/mL), High = HG + Zn-DHM (20 μg/mL). The error bars represent the means ± SDs (n = 3, ***P < 0.001, **P < 0.01, and *P < 0.05).

for 48 h induced high levels of intracellular ROS production in HUVECs, and owing to the antioxidant and SOD-like enzyme activities of the Zn-DHM NPs themselves, a significant reduction in intracellular ROS was observed when HG was added to the medium in a concentration-dependent manner (Fig. 4B and F). To further investigate the mechanism of ROS scavenging by Zn-DHM NPs, SOD and CAT kits were used, and the results revealed that the intracellular activities of the two enzymes were significantly reduced after HG treatment, whereas the addition of Zn-DHM NPs increased the intracellular activities of SOD and CAT in a concentration-dependent manner (Fig. 4G and H), possibly because Zn^{2+} is involved in the synthesis of enzymes [44]. Increased SOD enzyme activity accelerates the catalysis of $\cdot O_2$- to generate H_2O_2 and O_2, whereas elevated CAT activity accelerates the catalysis of H_2O_2 to generate H_2O and O_2, a cascade of catalytic reactions that can effectively scavenge ROS. Owing to excess ROS production and reduced antioxidant enzyme activity, in a high-glucose environment, the opening of the mitochondrial permeability transition pore (MPTP), positive ions or protons of the membrane interstitial space enter the matrix, resulting in the disappearance of the ionic gradient on both sides of the inner membrane, which in turn affects mitochondrial function [45]. JC-1 staining experiments revealed that when HUVECs were subjected to HG treatment for 48 h, the mitochondrial membrane potential decreased, JC-1 was detected as a monomer and emitted green fluorescence, whereas the mitochondrial membrane potential of the cells was maintained at a certain level after Zn-DHM NP treatment, and JC-1 formed J-aggregates and emitted red fluorescence (Fig. 4C). Mitochondrial dysfunction leads to apoptosis, and AM/PI fluorescence revealed that many dead cells were present in the field of view after treatment with HG for 48 h, whereas treatment with Zn-DHM NPs increased the number of live cells with increasing concentrations (Fig. 4D). Further verification via the Annexin V/PI flow assay revealed that the proportion of prematurely apoptotic cells accounted for 17.2 % of the total cells and only 70.2 % of the live cells after 48 h of HG treatment, whereas the proportion of apoptotic cells gradually decreased, and the proportion of live cells gradually increased after treatment with low and high concentrations of Zn-DHM NPs (Fig. 4E). We detected the apoptosis of L929 cells via the Annexin V/PI flow assay, and the results showed that Zn-DHM NPs also had protective effects on L929 cells (Fig. S7).

The above experimental results indicate that Zn-DHM NPs can effectively slow the oxidative stress induced by HG and protect mitochondrial function, which has great potential for inhibiting the development of diabetic wounds into difficult-to-heal wounds.

2.5. Zn-DHM NPs regulate HG-induced disorders of glucose metabolism

Eighty-five percent of the metabolic energy of HUVECs is derived from glycolysis, and moderate glycolysis facilitates vascular sprouting and neogenesis [46]. However, owing to the addiction of HUVECs to glycolysis, they are unable to resist glucose, and their excessive uptake of glucose in a high-glucose environment leads to excessive glycolysis and an increase in the end-product lactate [47]. Moreover, excessive intermediates lead to increased bypass metabolism toward polyols, methylglyoxal, etc., causing increased production of byproducts such as AGEs and ROS and excessive activation of the AGE-RAGE signaling pathway. The accumulation of AGEs promotes oxidative stress and inflammation, leading to endothelial cell dysfunction and tissue acidification [47]. In addition, excessive binding of AGEs to RAGE stimulates calcium deposition in the extracellular matrix through a variety of mechanisms, leading to functional cell apoptosis and vascular calcification [48]. Therefore, maintaining metabolic homeostasis plays an important role in promoting the early healing of diabetic wounds.

To investigate whether Zn-DHM NPs could maintain the intracellular glucose level in a homeostatic state, glucose uptake (Fig. 5F), intracellular glucose (Fig. 5G), and lactate levels were tested (Fig. 5H), and the results revealed that glucose uptake and intracellular glucose levels clearly increased after HG treatment of HUVECs, accompanied by an increase in lactate production. In contrast, in the Zn-DHM-treated group, the uptake of glucose decreased as its concentration increased, increasing the intracellular glucose level to a steady state, which in turn led to a reduction in lactate release. These results demonstrated that Zn-DHM NPs could reduce excessive glucose uptake and maintain the homeostasis of the intracellular glucose level.

To investigate whether Zn-DHM NPs are able to regulate glucose metabolism disorders, the level of cellular glycolysis was assessed by using Seahorse to determine the extracellular acidification rate (ECAR) (Fig. 5B). Compared with that in the control group, the level of glycolysis (basal glycolysis) in the cells significantly increased after 48 h of HG treatment, whereas the level of glycolysis (basal glycolysis) in the cells in the group treated with the addition of Zn-DHM NPs significantly decreased with increasing concentration (Fig. 5C). The second addition of the drug oligomycin, which is an inhibitor of ATP synthase, inhibits mitochondrial ATP production, thus shifting energy production to the glycolytic pathway, and the maximum ECAR value reached by the cells was the glycolytic capacity. Compared with the control group, the HG-treated group presented the highest glycolytic capacity, and the glycolytic capacity decreased after Zn-DHM treatment (Fig. 5D). The third addition of 2-DG, which inhibits glycolysis by competitively binding to the hexokinase of the glycolytic pathway, caused a decrease in the ECAR, thus confirming that ECAR production in the experiment originated from the glycolytic pathway. The difference between glycolytic capacity and glycolysis is the glycolytic reserve, which reflects the ability of a cell to meet its energy requirements. The results revealed that the energy requirements of the cells increased significantly after HG treatment, while there was no significant difference between the Zn-DHM NP treatment group and the HG group, which proved that the Zn-DHM NPs did not reduce the energy requirements of the cells (Fig. 5E). There was no significant difference in the level of non-glycolytic acidification among the cells in each group (Fig. S8). These results suggest that Zn-DHM NPs reduce excessive glycolysis caused by HG, resulting in a reduction in end-product lactate production.

The results of the CCK8 activity assay confirmed that the activity of the cells was inhibited after 24 h of HG treatment and that the Zn-DHM NPs effectively inhibited HG injury in a concentration-dependent manner (Fig. 5K). The results of the transwell assay revealed that the migration ability of the cells was significantly reduced after 48 h of HG treatment, and the migration ability of the Zn-DHM NPs was restored (Fig. 5I and L). The results of the tube formation assay revealed that the cells were almost unable to form tubes after 48 h of HG treatment and that the presence of Zn-DHM NPs promoted the recovery of tube formation ability (Fig. 5J and M). In addition, we also performed wound healing experiments on HUVECs. The results revealed that the migration and proliferation of HUVECs were impaired under HG conditions, whereas Zn-DHM NPs restored their function (Fig. S9).

The above experimental results demonstrated that Zn-DHM NPs were able to inhibit excessive glucose uptake by HUVECs in the HG environment and maintain intracellular glucose homeostasis, thereby downregulating excessive glycolysis, resulting in a decrease in end-product lactate production, maintaining metabolic level homeostasis, and thus protecting cellular function (Fig. 5A).

To further validate the mechanism by which Zn-DHM NPs protect against HG injury to HUVECs, 3v3 samples from the HG and Zn-DHM NP groups were selected for this study, and eukaryotic RNA transcriptome sequencing was performed. Heatmaps were first constructed to show the DEGs between the HG and Zn-DHM-NP groups (Fig. 6A), and volcano maps were constructed via 1.2-fold difference analysis to show that 1717 genes were downregulated and 1498 genes were upregulated after Zn-DHM-NP treatment compared with those in the HG group (Fig. 6B). GO enrichment analysis revealed that the DEGs were involved mainly in the activities of antioxidant enzymes and the maintenance of glucose homeostasis; furthermore, Zn-DHM NPs increased intracellular antioxidant enzyme activities and maintained intracellular glucose levels (Fig. 6C). KEGG enrichment analysis revealed that Zn-DHM NP

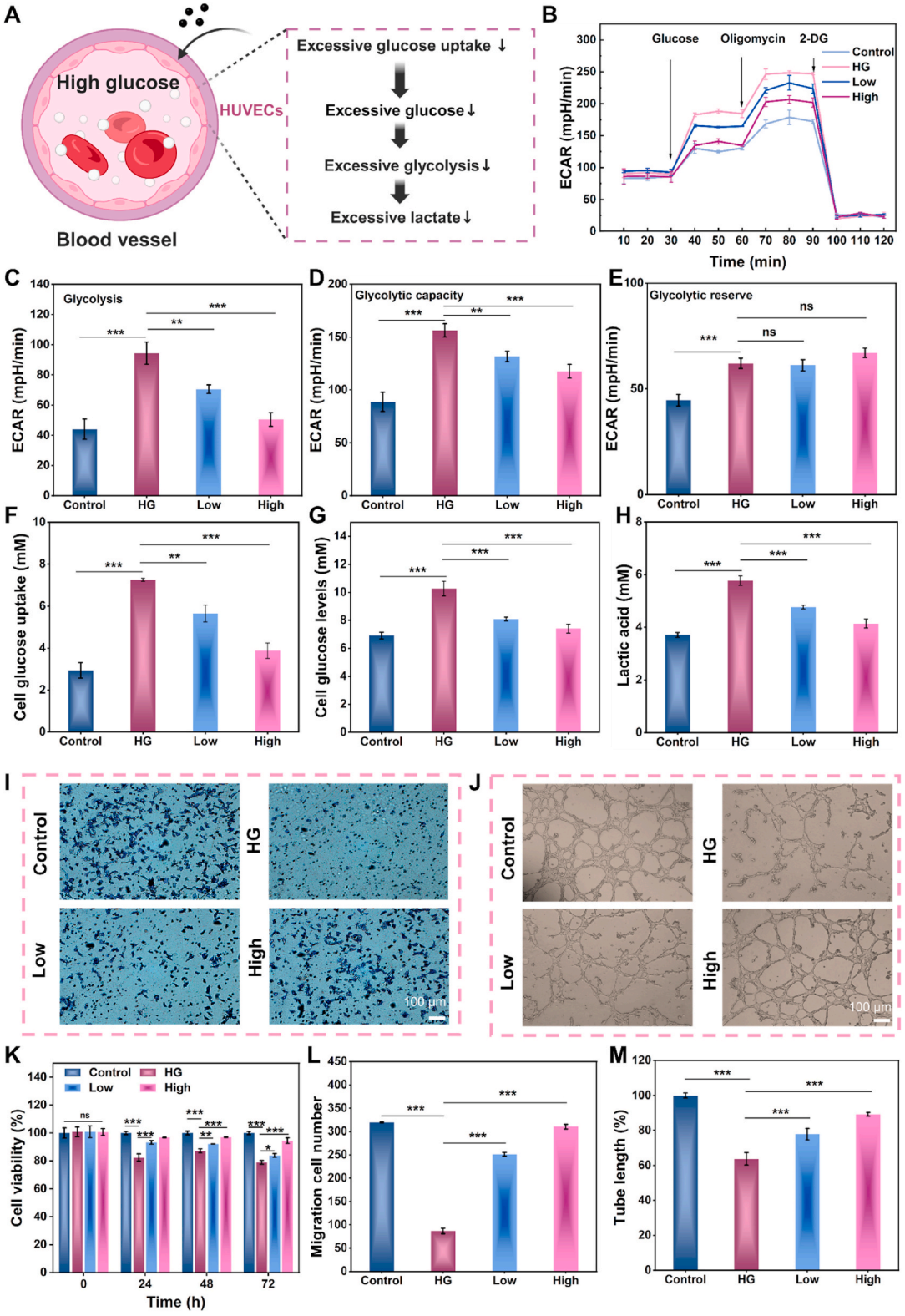

Fig. 5. Zn-DHM NPs regulate HG-induced disorders of glucose metabolism. (**A**) Mechanistic diagram of maintaining glucose homeostasis. (**B**) ECAR of different groups. (**C**) Glycolysis in the different groups. (**D**) Glycolytic capacity of the different groups. (**E**) Glycolytic reserves of the different groups. (**F**) Glucose uptake of different groups. (**G**) Glucose levels in cells in different groups. (**H**) Lactate levels in the cells of different groups. (**I, L**) Transwell analysis of HUVECs and statistical analysis via ImageJ. (**J, M**) Tube formation of HUVECs and statistical analysis by ImageJ. (**K**) CCK8 activity assay. The error bars represent the means ± SDs (n = 3, ***P < 0.001, **P < 0.01, and *P < 0.05).

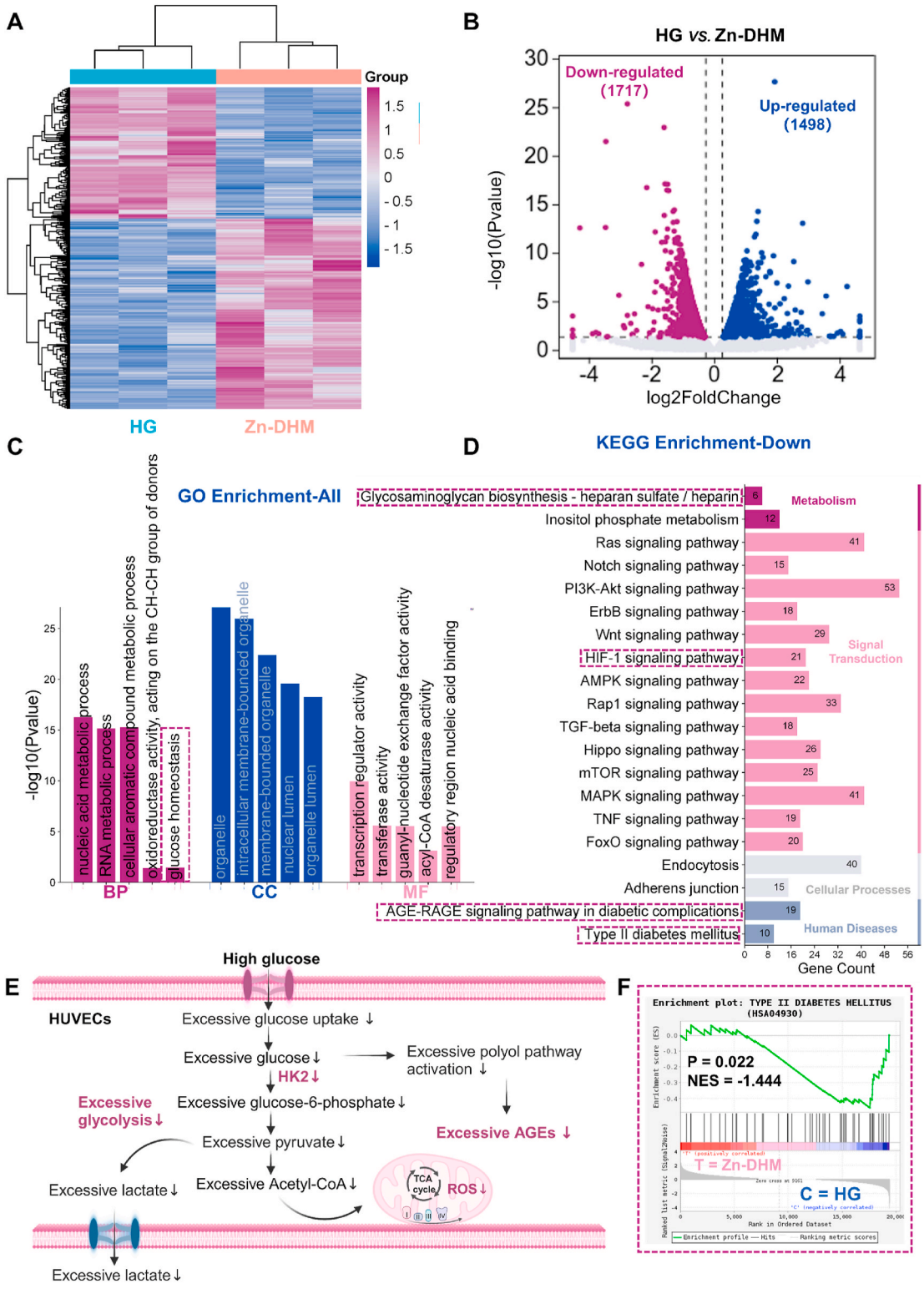

Fig. 6. RNA sequencing of HUVECs cultured with HG or Zn-DHM NPs. **(A)** Heatmap of significantly downregulated and upregulated genes after Zn-DHM NP treatment **(n = 3)**. **(B)** Volcano maps of genes after Zn-DHM NP treatment. **(C)** GO enrichment-All. **(D)** KEGG enrichment-down after Zn-DHM NP treatment. **(E)** The mechanism by which Zn-DHM NPs maintain glucose homeostasis. **(F)** GSEA revealed that some genes of the type 2 diabetes-related pathway were downregulated after Zn-DHM NP treatment.

treatment significantly downregulated the HIF-1 signaling pathway, the AGE-RAGE signaling pathway and the type 2 diabetes-related pathway in HUVECs (Fig. 6D), and the downregulation of HK2 could be observed in each pathway. GSEA similarly confirmed the significant down-regulation of several genes in the type 2 diabetes-related pathway after Zn-DHM NP treatment ($p = 0.02$) (Fig. 6F), and the heatmap revealed significant downregulation of HK2 (Fig. S10). The RT−qPCR results verified the downregulation of the HK2 gene (Fig. S11). HK2 plays a key role in glycolysis. HK2 catalyzes the reaction of glucose with ATP to produce glucose-6-phosphate (G6P), which is the initial step of

glycolysis. The reaction is irreversible and is one of the key regulatory points of glycolysis, which determines whether glucose can enter the metabolic pathway [49]. The downregulation of HK2 indicates that Zn-DHM NPs inhibit excessive glycolysis not only by reducing excessive glucose uptake but also by lowering the level of HK2. This reduces the overproduction of the intermediate product AGE, downregulates the AGE-RAGE signaling pathway, reduces ROS production and apoptosis, and simultaneously reduces the release of the end-product lactic acid to avoid overacidification of tissues, which is conducive to the early healing of diabetic wounds (Fig. 6E).

2.6. Zn-DHM NPs downregulate M1/M2 macrophage numbers

Macrophages play an important role in wound healing [50,51]: in the hemostatic phase, successive waves of infiltrating monocytes influx into the blood clot, and these monocytes differentiate into macrophages

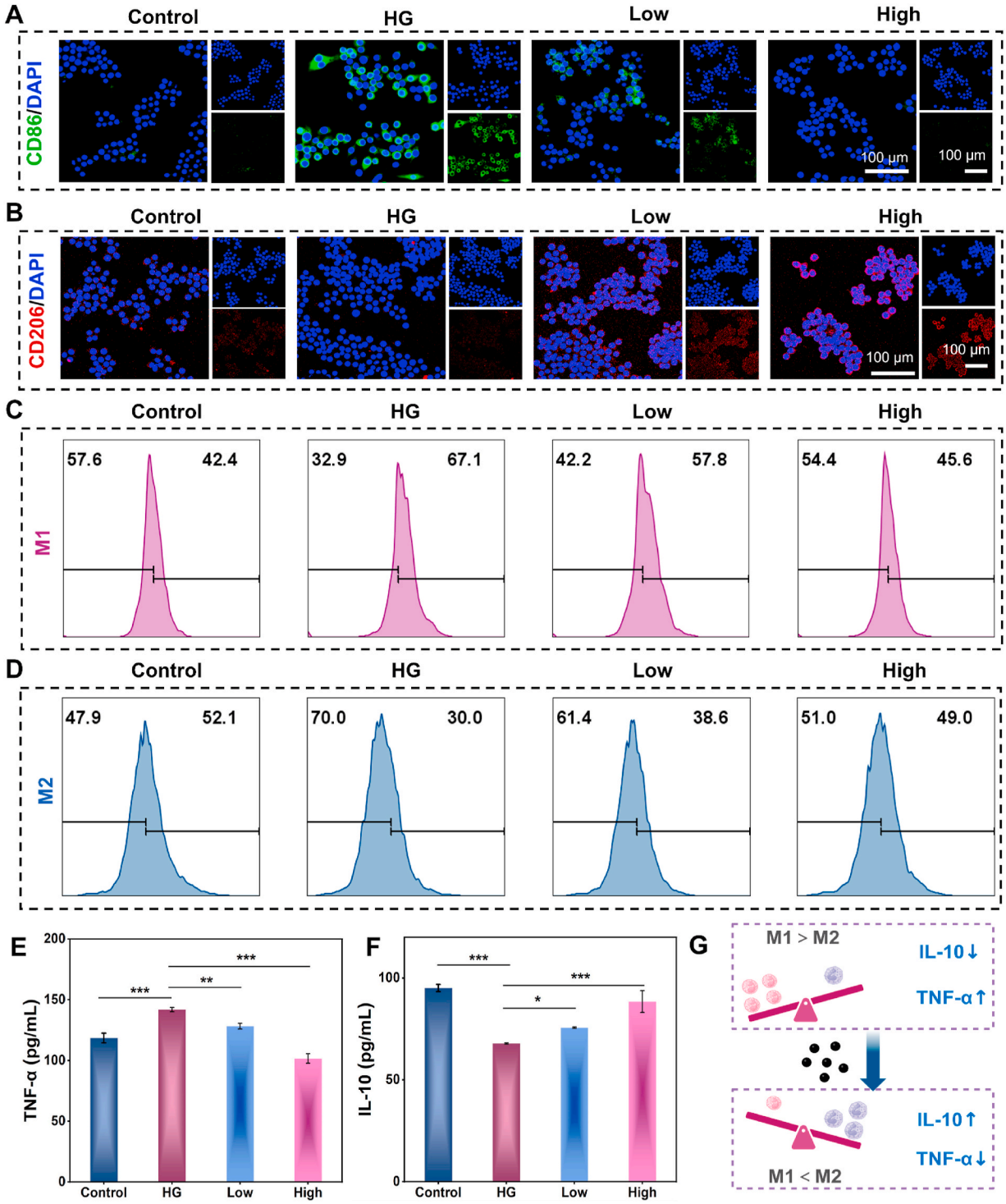

Fig. 7. Zn-DHM NPs decrease the M1/M2 macrophage ratio. (**A**) CD86 fluorescence staining. (**B**) CD206 fluorescence staining. (**C**) Flow assay for M1. (**D**) Flow cytometry assay for M2 macrophages. (**E**) ELISA for TNF-α. (**F**) ELISA for IL-10. (G) Mechanistic diagram of the decrease in the number of M1/M2 macrophages. The error bars represent the means ± SDs (n = 3, ***P < 0.001, **P < 0.01, and *P < 0.05).

in the wound; in the inflammatory phase, differentiated M1 macrophages scavenge pathogens and cellular debris and release NO, ROS, and proinflammatory cytokines, such as TNF-α and IL-6; during the proliferative phase, M2-type macrophages release cytokines such as IL-10 to promote tissue repair; and during the remodeling phase, macrophages release matrix metalloproteinases (MMPs) into the deposited ECM to complete healing with minimal scarring. However, in diabetic wounds, excessive oxidative stress and metabolic dysregulation due to the presence of high glucose increase macrophage polarization toward M1, which uses glycolysis as an energy source, and excessive ROS cause mitochondrial dysfunction, leading to a decrease in M2, which uses oxidative phosphorylation as an energy source, keeping the wound in the inflammatory phase and preventing it from entering the proliferative and remodeling phases [52]. Therefore, maintaining the homeostasis of M1/M2 macrophages is important for promoting early healing of diabetic wounds.

In this study, a model of HG-induced macrophage inflammatory polarization was established. CD86/206 fluorescence staining revealed that, compared with those in the control group, macrophages were more polarized toward M1 and less polarized toward M2 after 48 h of HG treatment, whereas with Zn-DHM NP treatment, macrophages gradually decreased their polarization toward M1 and increased their polarization toward M2 in a concentration-dependent manner (Fig. 7A and B). Flow cytometry data revealed that M0 macrophages polarized to the inflammatory M1 phenotype with glycolysis as the energy source after 48 h of high-glucose culture. After Zn-DHM NP treatment, the proportion of M0 to M1 polarization was significantly lower but still greater than that of the control group, indicating that Zn-DHM NPs maintained only M1/M2 homeostasis (Fig. 7C and D). To further investigate the ability of Zn-DHM NPs to regulate cytokine secretion by macrophages, ELISA was used, and the results revealed that, compared with macrophages cultured in normal glucose medium, macrophages in the HG-treated group secreted significantly greater levels of TNF-α and significantly lower levels of IL-10. The levels of TNF-α were significantly decreased,

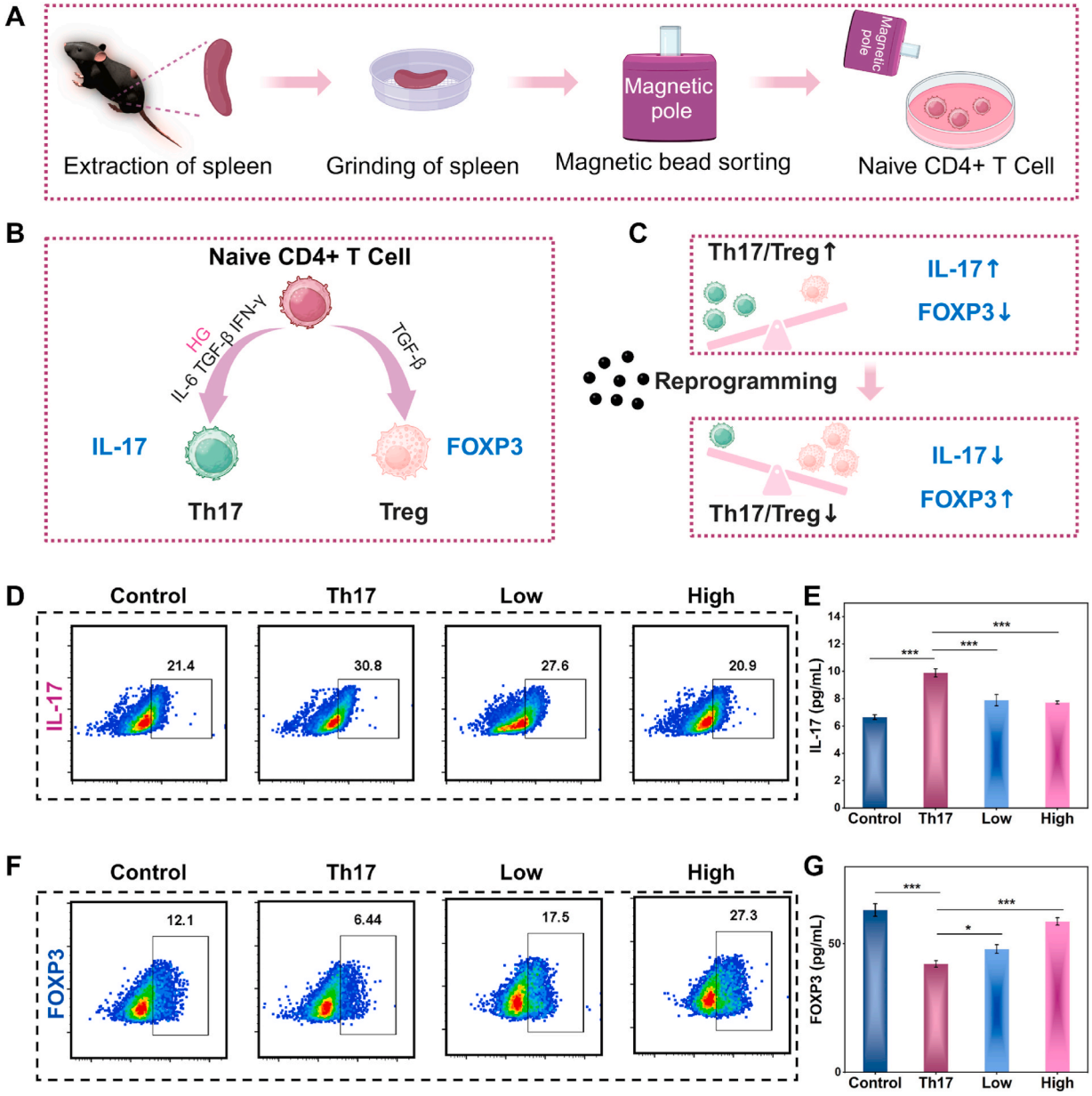

Fig. 8. Zn-DHM NPs decrease Th17/Treg levels and maintain homeostasis. (**A**) Mechanistic diagram of the extraction of naive $CD4^+$ T cells. (**B**) Mechanistic diagram of the Th17 polarization group. (**C**) Mechanistic diagram of the downregulation of Th17/Treg levels. (**D**) Flow assay for IL-17. (**E**) ELISA for IL-17. (**F**) Flow assay for FOXP3. (**G**) ELISA for FOXP3. The error bars represent the means ± SDs (n = 3, ***P < 0.001, **P < 0.01, and *P < 0.05).

and the levels of IL-10 were significantly increased after Zn-DHM NP treatment (Fig. 7E and F).

The above results indicated that in a HG environment, Zn-DHM NPs could downregulate macrophage M1/M2 levels, downregulate inflammatory factors, and upregulate anti-inflammatory factors (Fig. 7G), accelerating the progression of wounds from the inflammatory phase to the proliferative phase and thus achieving early healing.

2.7. Zn-DHM NPs decrease Th17/Treg levels and maintain homeostasis

Under prolonged hyperglycemic conditions, the release of various cytokines leads to high levels of polarization of naive $CD4^+$ T cells toward Th17/Treg cells [53,54]. IL-17 is the major factor that releases Th17 cells, and excessive IL-17 release leads to overactivation of the proinflammatory IL-17 signaling pathway [55]. In addition to aggravating inflammation, the released MMP9 released into the extracellular matrix excessively breaks down collagen and other factors that promote wound repair, leading to slower wound healing [56]. FOXP3 is a major transcription factor of Tregs that plays an important role in maintaining the balance of the immune system and suppressing inappropriate immune responses, and decreased levels of FOXP3 lead to immune dysregulation [57]. Therefore, maintaining Th17/Treg levels at homeostasis accelerates diabetic wound healing.

In this study, mouse spleens were first extracted for grinding, and naive $CD4^+$ T cells were extracted with magnetic beads and then expanded and activated with a CD3/28 antibody to obtain cells with the ability to polarize into Th17 and Treg cells (Fig. 8A). Then, HG, IL-6, TGF-β and IFN-γ were added to the culture medium to establish naive $CD4^+$ T cells for Th17 polarization (Fig. 8B), while Zn-DHM NPs were added to observe their ability to modulate naive $CD4^+$ T-cell polarization toward Th17/Treg cells. Compared with that in the control group, the level of IL-17 was significantly greater in the Th17-polarized group, which confirmed that the model was successfully established, whereas the level of IL-17 gradually decreased with increasing concentrations of Zn-DHM NPs (Fig. 8D). Compared with that in the control group, the level of FOXP3 was significantly lower in the Th17-polarized group, while the level of FOXP3 gradually increased with increasing concentrations of Zn-DHM NPs (Fig. 8F). To further investigate the ability of Zn-DHM NPs to regulate the polarization of naive $CD4^+$ T cells, the ELISA results revealed that, compared with the control group, the polarized group secreted a significantly greater level of IL-17 and a significantly lower level of FOXP3. The level of IL-17 was significantly decreased, and the level of FOXP3 was significantly increased after Zn-DHM NP treatment (Fig. 8E and G). The RT−qPCR results revealed that IL-17a was downregulated and that FOXP3 was upregulated after Zn-DHM NP treatment, which further verified the reliability of the conclusion (Fig. S12). The reason why Zn-DHM NPs regulate the Th17/Treg balance may be related to the alleviation of oxidative stress and the supplementation of an appropriate amount of Zn ions [58].

The above results indicated that Zn-DHM NPs could maintain Th17/Treg homeostasis, downregulate the IL-17 signaling pathway to reduce inflammation, and upregulate FOXP3 to maintain immune homeostasis, thus promoting early wound healing in diabetic mice (Fig. 8C).

2.8. Zn-DHM NPs promote early wound healing in diabetic mice

In this study, a type 2 diabetic mouse wound model was established to investigate the ability of Zn-DHM NPs to promote early diabetic wound healing. To simulate a clinical surgical scenario, the mice were prepared for skinning one day prior to modeling and were administered on the day of modeling and the following two days, and photographs of the wounds were taken on days 4, 7 and 10, with samples ultimately collected on day 14 for H&E, Masson, immunohistochemistry, and RNA sequencing analyses (Fig. 9A).

Photographic recordings of the wounds of the mice revealed that the control group had the slowest degree of wound healing, with some inflammatory secretions visible oozing from the surface. DHM, $ZnCl_2$ and Zn-DHM promoted wound healing, but the Zn-DHM group presented the best results, with almost complete wound healing on day 14 and the presence of new hairs on the surface of the new skin (Fig. 9B and C). An analysis of the wound area via ImageJ revealed that the Zn-DHM NP healing rate was as high as 99.70 % on day 14, which was significantly greater than that of the other groups (Fig. 9D). After several blood glucose measurements during the modeling period, all four groups of mice maintained high blood glucose levels without significant differences, indicating stable modeling (Fig. 9E), and the body weights of the four groups of mice likewise did not significantly differ (Fig. 9F), which ruled out chance.

The results of H&E staining revealed that a large amount of inflammatory cell infiltration was visible during the trauma of the control group, with no obvious granulation tissue or neovascularization (Fig. S13). A moderate amount of inflammatory cell infiltration was visible in both the DHM and $ZnCl_2$ groups, and better proneovascularization was observed in the $ZnCl_2$ group than in the DHM group. A large amount of neovascularization and granulation tissue was visible upon trauma in the Zn-DHM NP group, with only a small number of infiltrating inflammatory cells and many hair follicles and glands. The wounds were basically healed, and the effect was greater than that in the DHM and $ZnCl_2$ groups (Fig. 9G, Fig. S14). The Masson results revealed that the wounds in the Zn-DHM NP group had well-arranged fibrotic tissues accompanied by neocollagenesis, whereas the wounds in the control group had only a small amount of neocollagenesis, and the fibrotic tissues were poorly aligned (Fig. 9H, Fig. S15). The results of H&E and Masson staining revealed that Zn-DHM NPs effectively reduced inflammation in diabetic wounds and promoted neovascularization, granulation and collagen formation, thus transitioning from the inflammatory phase to the proliferative phase and accelerating healing during the remodeling period.

To further investigate the mechanism by which Zn-DHM NPs promote diabetic wound healing *in vivo*, immunohistochemical (IHC) assays were performed on wound samples. Compared with those in the control group, the ROS levels in the wounds were significantly lower in the Zn-DHM NP-treated group (Fig. 10A and G), which demonstrated that the Zn-DHM NPs still have superior antioxidant capacity *in vivo*. This disrupts the ROS-inflammatory cascade cycle, resulting in a reduction in the release of inflammatory factors such as TNF-α (Fig. 10E and K) and MMP9 (Fig. 10F and L). The clearance of excess ROS and the reduced release of inflammatory factors led to a reduction in apoptosis. Compared with the control, Zn-DHM NPs significantly decreased the level of caspase-3 (Fig. 10D and J), which, as a member of the cysteine enzyme family, is a key executor of apoptosis, and a reduction in its level leads to a reduction in the occurrence of apoptosis. Compared with the control, Zn-DHM NPs significantly increased the levels of VEGF (Fig. 10B and H) and CD31 (Fig. 10C and I) in the wounds, suggesting that Zn-DHM NPs still have superior proangiogenic ability *in vivo*. In addition, immune-related indices were examined in the wound samples. CD206/iNOS fluorescence staining revealed that Zn-DHM NPs still had the ability to regulate the direction of macrophage polarization *in vivo*, which could reduce the number of M1/M2 macrophages in the wounds, thus reducing the release of the inflammatory factor TNF-α and promoting tissue repair (Fig. 11A and D). IL-17 fluorescence staining revealed that Zn-DHM NPs still had the ability to downregulate naive $CD4^+$ T-cell polarization toward Th17 cells *in vivo* (Fig. 11B and E), thereby inhibiting the overactivation of IL-17 signaling channels, reducing the excessive release of MMP9, and cleaving collagen during remodeling to complete skin healing [59]. FOXP3 fluorescence staining revealed that Zn-DHM NPs still had the ability to increase naive $CD4^+$ T-cell polarization toward Treg cells, and the upregulation of FOXP3 was beneficial for maintaining immune homeostasis and promoting early wound healing (Fig. 11C and F).

To further validate the mechanism by which Zn-DHM NPs promote diabetic wound healing *in vivo*, in this study, we chose control and Zn-

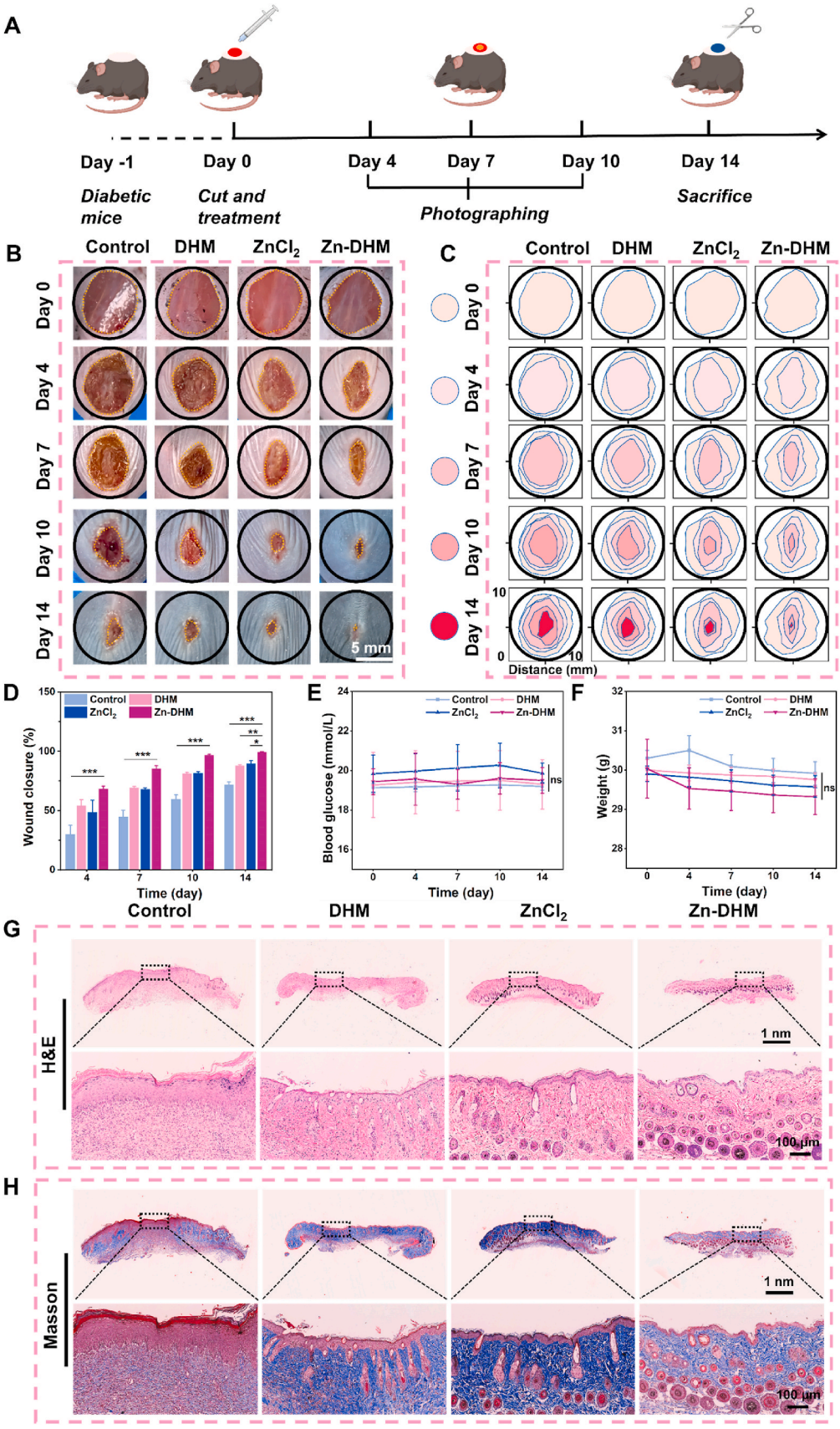

Fig. 9. Zn-DHM NPs promote early wound healing in diabetic mice (A) Mechanistic diagram of the construction of the diabetic mouse wound model. (**B-C**) Photos and areas of wounds on days 0, 4, 7, 10, and 14. (**D**) Wound healing rates of diabetic mice on days 4, 7, 10, and 14. (**E**) Blood glucose. (**F**) Weight. (**G**) H&E staining on day 14. (**H**) Masson staining on day 14. The error bars represent the means ± SDs (n = 3, ***P < 0.001, **P < 0.01, and *P < 0.05).

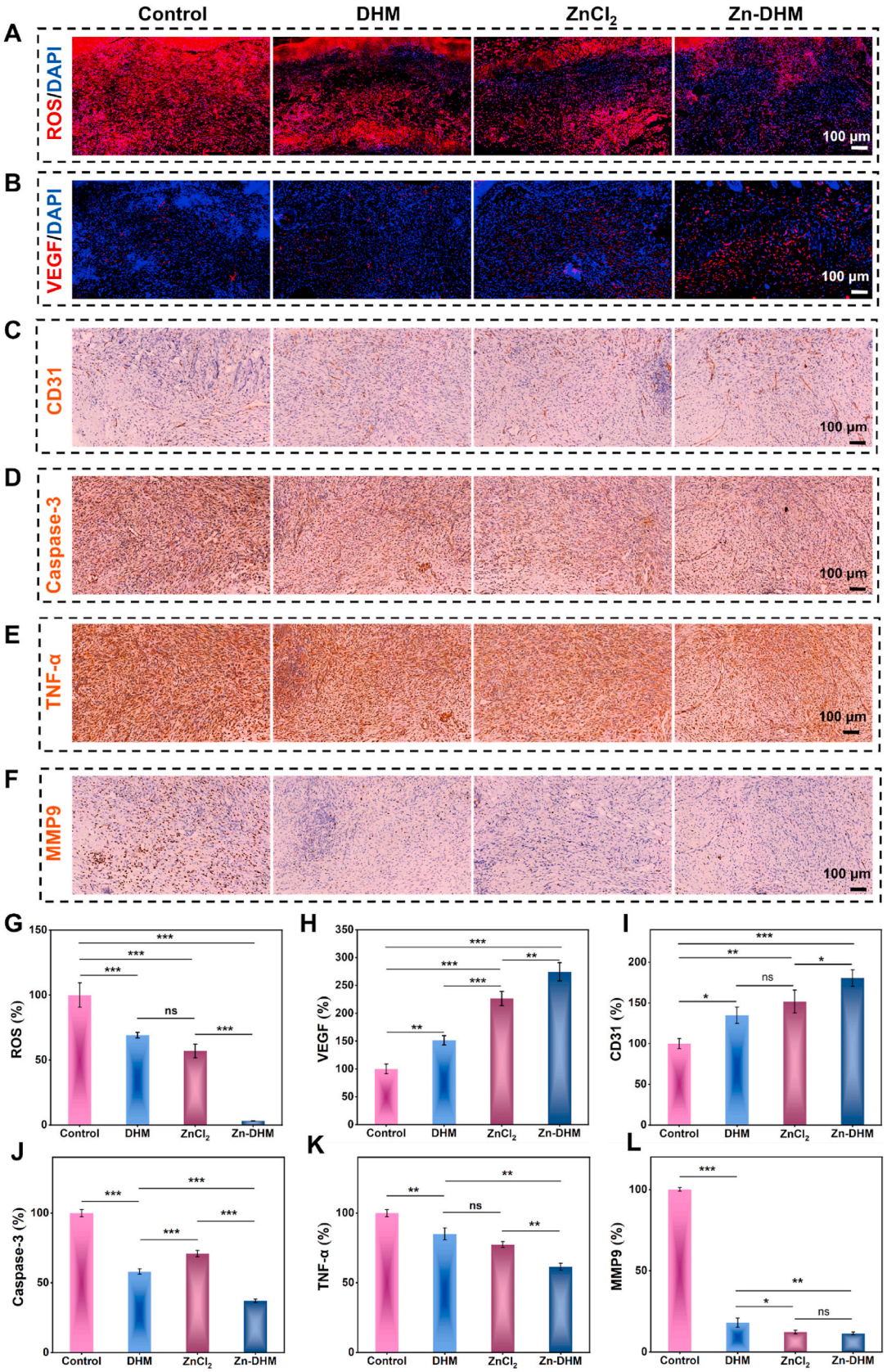

Fig. 10. Zn-DHM NPs scavenge ROS and have anti-inflammatory, antiapoptotic and proangiogenic effects *in vivo*. (**A, G**) Immunofluorescence analysis of ROS and statistical analysis. (**B, H**) Immunofluorescence analysis of VEGF and statistical analysis. (**C, I**) IHC for CD31 and statistical analysis. (**D, J**) IHC analysis of Caspase-3 expression and statistical analysis. (**E, K**) IHC for TNF-α and statistical analysis. (**F, L**) IHC for MMP9 and statistical analysis. The error bars represent the means ± SDs (n = 3, ***P < 0.001, **P < 0.01, and *P < 0.05).

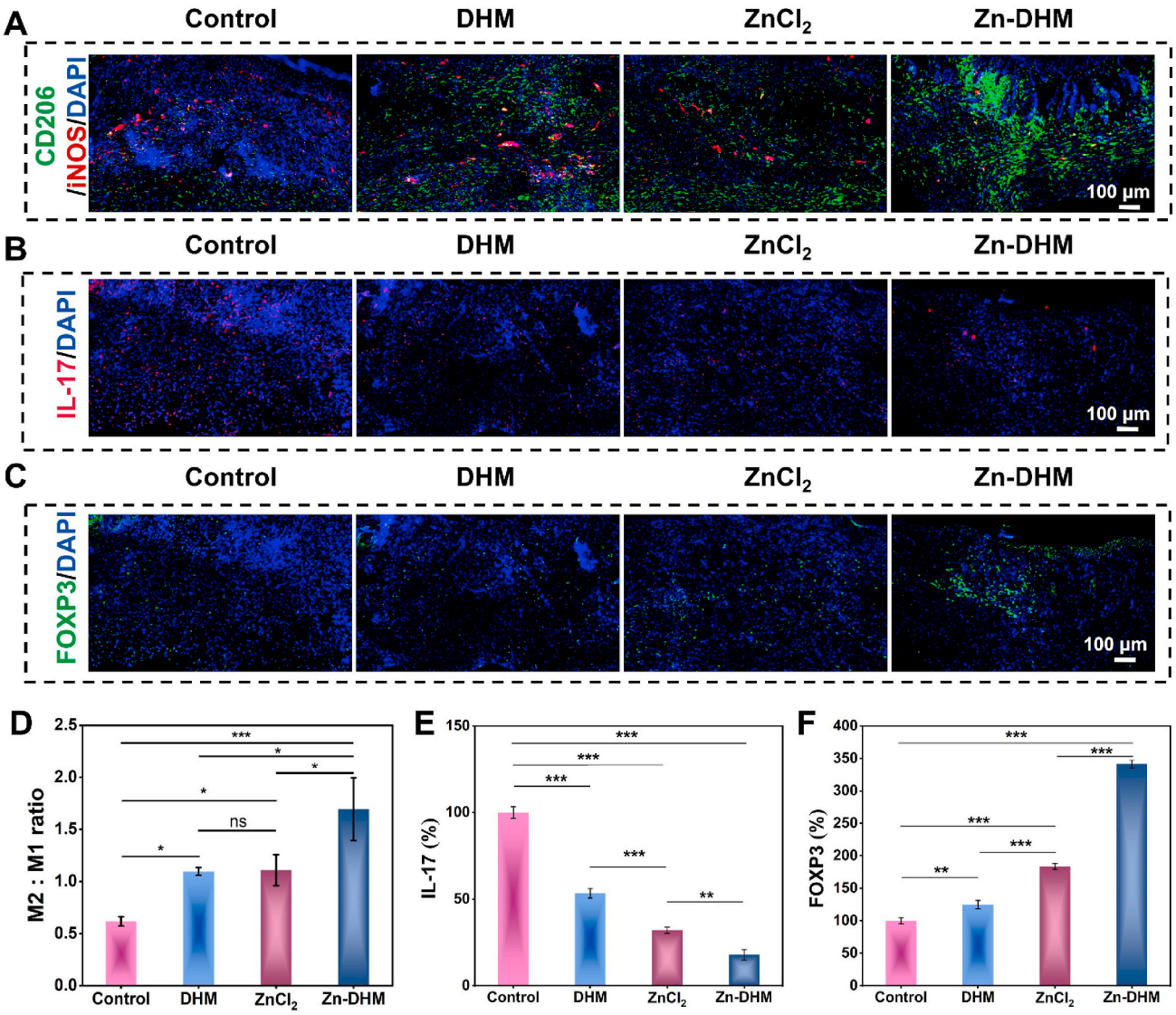

Fig. 11. Zn-DHM NPs maintain immune homeostasis *in vivo*. (**A**) Immunofluorescence of CD206/iNOS. (**B**) Immunofluorescence of IL-17. (**C**) Immunofluorescence of FOXP3. (**D**) Statistical analysis of M2:M1 expression via ImageJ. (**E**) Statistical analysis of IL-17 expression via ImageJ. (**F**) Statistical analysis of FOXP3 expression via ImageJ. The error bars represent the means ± SDs (n = 3, ***P < 0.001, **P < 0.01, and *P < 0.05).

DHM NP groups of wound samples and performed eukaryotic RNA transcriptome 3v3 sequencing. A heatmap was first constructed to demonstrate the DEGs between the control and Zn-DHM-NP groups (Fig. 12A), and a volcano map was constructed via 1.2-fold difference analysis to show that 999 genes were downregulated and that 884 genes were upregulated in the Zn-DHM-NP group compared with the control group (Fig. 12B). GO enrichment analysis revealed that the DEGs were enriched mainly in genes related to tissue regeneration, immune modulation, metabolic regulation and homeostasis (Fig. 12C), especially those related to the differentiation of macrophages and Th17 cells (Fig. 12I). KEGG enrichment analysis revealed that Zn-DHM NPs significantly downregulated the HIF-1 signaling pathway, the AGE-RAGE signaling pathway, the IL-17 signaling pathway and apoptosis (Fig. 12D), which reduced the release of inflammatory factors and played an anti-inflammatory role (Fig. 12H). GSEA revealed that the Zn-DHM NPs still had a protective effect on mitochondrial function *in vivo*, accelerating DNA repair (Fig. 12F) and promoting cell proliferation (Fig. 12G) by upregulating the TCA cycle (Fig. 12E).

2.9. Zn-DHM NPs have good biosafety in vivo

To investigate the biosafety of the Zn-DHM NPs *in vivo*, H&E staining was performed on the heart, liver, spleen, lung, kidney and other organs of the four groups of mice, which revealed that there was no significant difference in the histomorphology of the organs in the four groups and that there was no obvious toxicity of the Zn-DHM NPs to the organs (Fig. S16). The results of routine blood and biochemical analyses revealed that these parameters were basically within the normal physiological range for the routine blood parameters (Fig. S17) or biochemical indices (Fig. S18) of the four groups of mice. These results indicate that Zn-DHM NPs have good biological safety *in vivo*.

3. Conclusion

In this study, a novel metal–polyphenolic nanozyme (Zn-DHM NPs) that is homogeneous in size and structurally stable was successfully synthesized. It possesses the properties of Zn^{2+} and DHM, which not only scavenge ROS and promote cell proliferation and migration but also regulate metabolism and immune homeostasis. This reduces inflammation and accelerates the transition of diabetic wounds from the

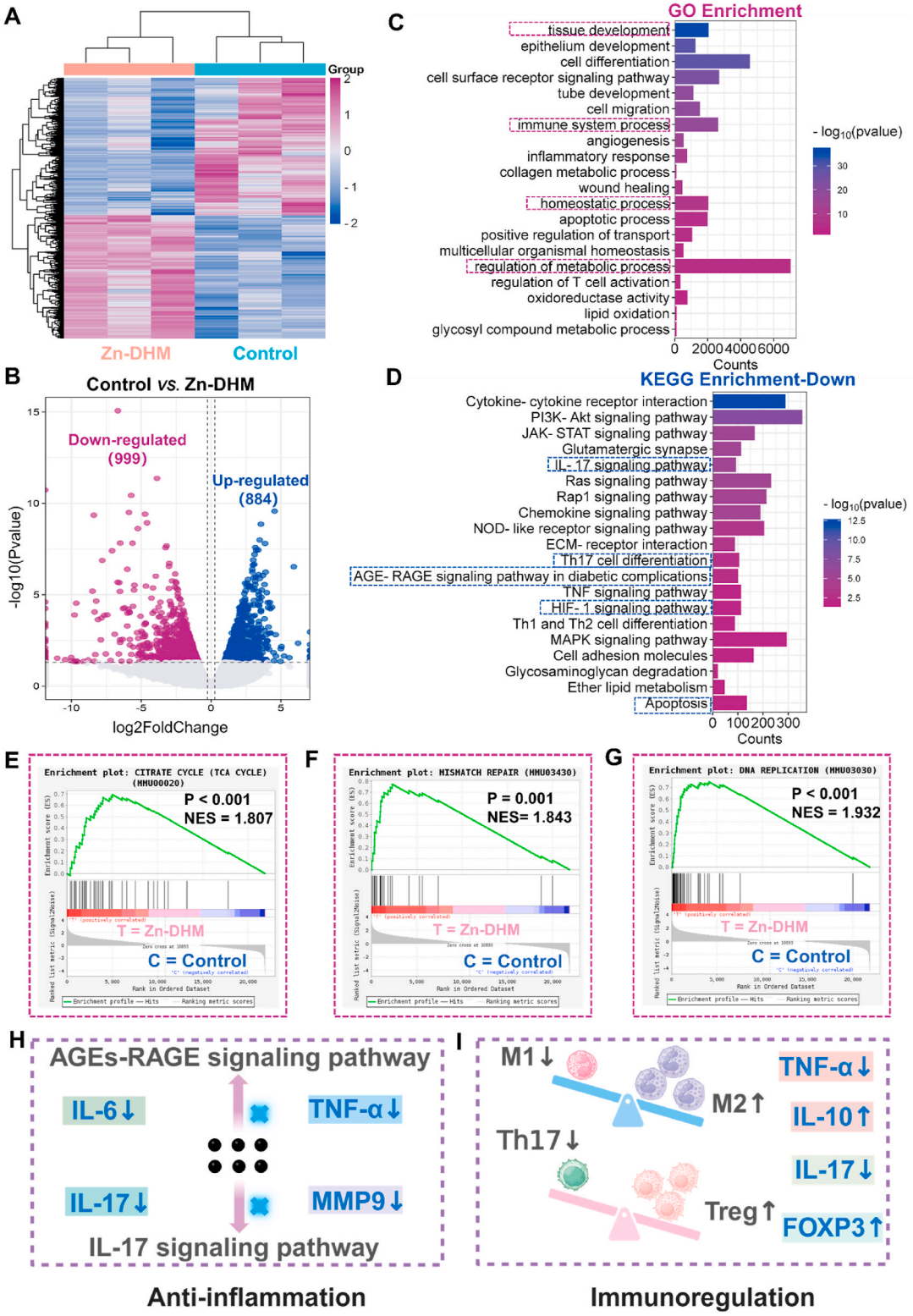

Fig. 12. RNA sequencing of wound samples from the control and Zn-DHM NP groups. (**A**) Heatmap of significantly downregulated and upregulated genes after Zn-DHM NP treatment (**n = 3**). (**B**) Volcano maps of genes after Zn-DHM NP treatment. (**C**) GO enrichment-All. (**D**) KEGG enrichment-down after Zn-DHM NP treatment. (**E-G**) GSEA revealed that several genes associated with the TCA cycle, DNA repair and DNA replication were upregulated after Zn-DHM NP treatment. (**H**) The mechanism of the anti-inflammatory effects *in vivo*. (**I**) The mechanism of immunoregulation *in vivo*.

inflammatory phase to the proliferative phase. *In vitro/in vivo* experiments and RNA sequencing analyses revealed that Zn-DHM NPs not only possess antioxidant properties but also increase the levels of intracellular SOD and CAT to scavenge ROS and maintain the level of the MMP to reduce apoptosis. In terms of glucose metabolism, Zn-DHM NPs reduce the excessive uptake of glucose by HUVECs and downregulate the intracellular glucose and HK2 levels, thus inhibiting excessive glycolysis. It reduces the production of the end product lactate and

intermediate AGE, which in turn downregulates the AGE-RAGE pathway, slows oxidative stress and inflammation, and restores cellular function. In terms of immune regulation, on the one hand, Zn-DHM NPS was able to downregulate M1/M2 levels, reduce the release of inflammatory factors and increase the release of anti-inflammatory factors and factors promoting tissue repair, thus promoting wound repair. On the other hand, it can downregulate Th17/Treg levels and inhibit overactivation of the IL-17 signaling pathway, thereby reducing the release of inflammatory factors and MMP9 and promoting collagen formation in the remodeling phase and epithelialization. The upregulation of FOXP3 facilitated the maintenance of immune homeostasis, thereby promoting early wound healing in diabetic mice. Notably, Zn-DHM NPs also have a favorable biosafety profile. In conclusion, the development of Zn-DHM NPs provides a new target for the treatment of early diabetic wounds.

4. Materials and methods

4.1. Materials and reagents

$ZnCl_2$ (7646-85-7), DHM (27200-12-0), PVP (9003-39-8), Methano (67-56-1), and N,N-dimethylformamide (DMF) (68-12-2) (Shanghai, China, Aladdin Co., Ltd.) were used. 2,2-Biazobis(3-ethyl-benzothiazole-6-sulfonic acid) diammonium salt (ABTS) (30931-67-0), 1,1-diphenyl-2-trinitrophenylhydrazine (DPPH) (1898-4), 2-phenyl-4,4,5,5-tetramethylimidazolidine-3-oxo-1-oxo (PTIO) (18390-6), 3,3′,5,5′-tetramethylbenzene diamine (TMB) (54827-17-7), ferrous sulfate (FeSO4-7H2O) (7782-63-0) (Chongqing, China, Macklin Biochemical Co.) H_2O_2 (7722-84-1) (Sichuan, China, XiLong Scientific Co., Ltd.); SOD assay kit (S0101-3), Cell Counting Kit-8 (CCK-8) (CT0001-B), STZ (SJ-MA0060) (Shandong Sparkjade Biotechnology Co., Ltd.); apoptosis assay kit (BB-4101), (Shanghai, China, Bestbio Co., Ltd.); and ROS assay kit (S0033M), JC-8)

Enzyme-linked immunosorbent assay (ELISA) kits for IL-10 (JL20242), TNF-α (JL10484), IL-17 (JLW20251), and FOXP3 (JL20288) (Shanghai, China; Jianglai Biology Co., Ltd.); inducible nitric oxide synthase (iNOS) antibodies (AF0199), CD206 (DF4169), caspase-3 (AF7022), VEGF (AF5131), CD31 (AF6191), TNF-α (AF7014), and MMP9 (AF5228) antibodies for immunohistochemistry (IHC) (Changzhou, China; Affinity Co., Ltd.); and human umbilical vein endothelial cells (HUVECs), mouse macrophages (RAW 264.7 cells) and L929 cells were purchased from Pronosay (Wuhan, China). C57BL/6 mice were purchased from Skibbes Animals (Henan, China).

4.2. Synthesis of Zn-DHM NPs

First, 330 mg of PVP was dissolved in 25 mL of MD organic mixed solvent (Methano:DMF = 1:1), and then 100 mg of $ZnCl_2$ solid was fully dissolved in 5 mL of MD solvent, which was slowly added to the PVP solution. After magnetic stirring for 20 min, 50 mg of DHM was dissolved in 5 mL of MD solvent and added slowly dropwise to the reaction mixture with sufficient stirring for 24 h. Finally, the reacted mixture was put into a dialysis bag with a molecular weight of 8000–14,000 KD for 24 h to produce a solution of Zn-DHM NPs, which solidified overnight at −80 °C and then put into a vacuum lyophilizer for 24 h to produce the Zn-DHM NP powder.

4.3. Characterization of Zn-DHM NPs

The Zn content in the samples was quantified via inductively coupled plasma emission spectrometry (ICP−OES) (Puyu Technology, EXPEC 6500, Hangzhou, China); the morphological features of the Zn-DHM NPs were observed via transmission electron microscopy (TEM) (Thermo Scientific, Talos L120C G2, Beijing, China); the nanoparticle size and zeta potential analyzer were used to measure the particle size and zeta potential of the Zn-DHM NPs (NanoBrook, 90Plus PALS, Shanghai, China); X-ray photoelectron spectroscopy (XPS) was used to understand the elemental composition of the Zn-DHM NPs, the chemical state of each element and the chemical bond distribution (Thermo Scientific, K-Alpha, Beijing, China); X-ray diffraction (XRD) was used to understand the crystal structure of the Zn-DHM NPs (Bruker, D8 ADVANCE, Beijing, China); and the functional groups of the Zn-DHM NPs were determined via Fourier transform infrared spectroscopy (FTIR) (Yingsa Optics, FOLI20, Shanghai, China).

4.4. In vitro assessment of the antioxidant capacity and enzyme-like activity of Zn-DHM NPs

The redox properties of the Zn-DHM NPs were clarified by probing experiments, such as $ABTS^{\cdot+}$, DPPH·, PTIO· and TMB scavenging, to explore their ability to scavenge ROS/RNS and their scavenging efficiency. The SOD activity of the Zn-DHM NPs was measured to clarify the enzyme-like nature and antioxidant products of the Zn-DHM NPs to elucidate the mechanism and principle of ROS scavenging by the Zn-DHM NPs.

4.5. Cell culture

HUVECs, L929 cells, RAW 264.7 cells and naive $CD4^+$ T cells were used in this study for *in vitro* experiments. HUVECs were cultured in endothelial cell-specific medium (ECM); L929 cells were cultured in DMEM supplemented with 10 % fetal bovine serum, 100 U/mL penicillin and 100 U/mL streptomycin; RAW 264.7 cells were cultured in macrophage-specific medium; and naive $CD4^+$ T cells were cultured in RPMI-1640 medium supplemented with 10 % fetal bovine serum, 100 U/mL penicillin, and 100 U/mL streptomycin. All the cells were cultured at 37 °C in a carbon dioxide incubator containing 5 % carbon dioxide. The medium and cell passages were changed according to the cell growth status.

4.6. Functional detection of Zn-DHM NPs in vitro

First, the toxic effects of different concentrations of materials on cells were detected via a CCK-8 kit, and then, suitable concentrations were selected for the CCK8 proliferation assay and Transwell assay to detect the ability of Zn-DHM NPs to promote the proliferation and migration of HUVECs. A tube formation assay of HUVECs and a scratch assay of L929 cells were used to detect the ability of Zn-DHM NPs and their components to promote angiogenesis and epithelialization.

4.7. Establishing a model of HUVECs injury by HG

By constructing a high-glucose (HG, 35 mM)-induced HUVEC injury model, the ability of Zn-DHM NPs to restore cell proliferation, migration and angiogenesis in HG-injured cells was examined via a CCK-8 kit, a transwell assay and a tube-forming assay, respectively; the ability of Zn-DHM NPs to clear ROS was examined via an ROS fluorescence staining kit; and the ability of Zn-DHM NPs to inhibit apoptosis and protect the mitochondrial membrane potential in response to HG injury was examined via an apoptosis kit, a live−dead cell staining kit, and a mitochondrial membrane potential assay kit (JC-1). The glucose metabolism level of HUVECs was assessed by detecting glucose uptake and intracellular glucose and lactate levels under HG conditions, while the ability of Zn-DHM NPs to regulate glucose metabolism was observed by detecting the extracellular acidification rate via a Seahorse XF system. RNA transcriptome sequencing was performed to further investigate the mechanism by which Zn-DHM NPs protect HUVECs from HG injury.

4.8. Model of HG-induced polarization of RAW264.7 cells toward the M1 phenotype

By constructing a model of HG-induced polarization of RAW264.7

cells toward M1, the ability of Zn-DHM NPs to regulate the macrophage phenotype was detected via an INOS Immunofluorescence Staining Kit and a CD206 Immunofluorescence Staining Kit, and the ability of Zn-DHM NPs to inhibit the release of inflammatory factors was detected via TNF-α and IL-10 enzyme immunoassay kits.

4.9. Model of the polarization of naive $CD4^+$ T cells toward Th17 cells

The suspended cells were first prepared by grinding the spleens extracted from the mice, and then a stem cell sorting kit was used to sort the naive $CD4^+$ T cells. The ability of the Zn-DHM NPs to regulate the polarization of naive $CD4^+$ T cells was investigated by polarizing naive $CD4^+$ T cells toward Th17 cells. The ability of Zn-DHM NPs to maintain Th17/Treg homeostasis was examined via IL-17 and FOXP3 flow cytometry and ELISA kits.

4.10. In vivo animal experiments

Thirty 5-week-old male C57BL/6J mice were selected, and after one week of acclimatization, they were changed to high-sugar or high-fat chow for 6 w. Mice were continuously injected intraperitoneally with STZ solution for 5 d. Successful diabetic mice were randomly divided into four groups of five mice each, i.e., the PBS (Control) group, the $ZnCl_2$ group, the DHM group, and the Zn-DHM NP treatment group. The dorsal cuts were approximately 1 cm in diameter, and the groups were treated medically. To systematically evaluate the ability of Zn-DHM NPs to promote the healing of diabetic wounds *in vivo*, mice were observed after different treatments, and the healing of the wounds was recorded on days 0, 4, 7, 10, and 14. At the end of treatment, H&E and Masson staining and IHC staining of the wounds were performed to assess angiogenesis, apoptosis, inflammatory status, macrophage phenotype and Th17/Treg levels. The mechanism was further validated via RNA transcriptome sequencing of fresh samples.

4.11. In vivo biosafety evaluation

To determine whether Zn-DHM NPs have good physiological stability and excellent biocompatibility, they were systematically evaluated via histological sections of heart, liver, spleen, lung and kidney organs and hematological indices in animals.

4.12. Statistical analysis

GraphPad Prism 8.0 software was used for all the statistical calculations. The results are shown as the mean ± standard deviation (SD) of at least three replicates of each experiment. Statistical significance was analyzed via Student's *t*-test (two groups), one-way ANOVA or two-way ANOVA with Tukey's multiple comparisons test (over two groups). P values of 0.05 or less were considered significant (***$P < 0.001$, **$P < 0.01$, and *$P < 0.05$).

CRediT authorship contribution statement

Shuo Zhang: Writing – original draft, Visualization, Validation, Resources, Methodology, Investigation, Formal analysis, Conceptualization. **Xinyu Zhao:** Writing – original draft, Validation, Software, Methodology. **Wei Zhang:** Writing – original draft, Methodology. **Xiaolong Wei:** Visualization, Software, Resources, Methodology. **Xu-Lin Chen:** Visualization, Supervision, Resources, Investigation, Conceptualization. **Xianwen Wang:** Writing – review & editing, Visualization, Validation, Supervision, Methodology, Funding acquisition.

Ethics approval and consent to participate

All animal experiments were reviewed and approved by the Animal Care and Use Committee of Anhui Medical University (No. LLSC20220731).

Declartion of competing interest

The authors declare no conflicts of interest.

Acknowledgments

S. Zhang, X. Zhao and W. Zhang contributed equally to this work. This work was supported by the National Natural Science Foundation of China (82172204, 82372552, 82372517), the Anhui Key Research and Development Plan (Grant no. 202104j07020027), the Excellent Youth of Natural Science Research Projects in Anhui Province Universities (2023AH030060), the Anhui Provincial Natural Science Foundation (2408085Y016), and the Anhui Province Excellent Research and Innovation Team Project (2024AH010013). The authors would like to thank the Shiyan laboratory (www.shiyanjia.com) for their help in language polishing. Figures were created by Biorender (https://www.biorender.com).

Appendix A. Supplementary data

Supplementary data to this article can be found online at https://doi.org/10.1016/j.bioactmat.2025.02.041.

References

[1] Y. Li, D. Teng, X. Shi, G. Qin, Y. Qin, H. Quan, B. Shi, H. Sun, J. Ba, B. Chen, J. Du, L. He, X. Lai, Y. Li, H. Chi, E. Liao, C. Liu, L. Liu, X. Tang, N. Tong, G. Wang, J. A. Zhang, Y. Wang, Y. Xue, L. Yan, J. Yang, L. Yang, Y. Yao, Z. Ye, Q. Zhang, L. Zhang, J. Zhu, M. Zhu, G. Ning, Y. Mu, J. Zhao, W. Teng, Z. Shan, Prevalence of diabetes recorded in mainland China using 2018 diagnostic criteria from the American Diabetes Association: national cross sectional study, Bmj 369 (2020) m997.

[2] W. Dai, R. Shu, F. Yang, B. Li, H.M. Johnson, S. Yu, H. Yang, Y.K. Chan, W. Yang, D. Bai, Y. Deng, Engineered Bio-heterojunction confers extra- and intracellular bacterial ferroptosis and hunger-triggered cell protection for diabetic wound repair, Adv Mater 36 (9) (2024) e2305277.

[3] O.A. Peña, P. Martin, Cellular and molecular mechanisms of skin wound healing, Nat. Rev. Mol. Cell Biol. 25 (8) (2024) 599–616.

[4] M. He, Z. Wang, H. Yang, Q. Wang, D. Xiang, X. Pang, Y.K. Chan, D. Sun, G. Yin, W. Yang, Y. Deng, Multi-functional bio-HJzyme: revolutionizing diabetic skin regeneration with its glucose-unlocked sterilization and programmed anti-inflammatory effects, Adv. Sci. 10 (21) (2023) e2300986.

[5] J. Wang, X.Y. Chen, Y. Zhao, Y. Yang, W. Wang, C. Wu, B. Yang, Z. Zhang, L. Zhang, Y. Liu, X. Du, W. Li, L. Qiu, P. Jiang, X.Z. Mou, Y.Q. Li, pH-switchable antimicrobial nanofiber networks of hydrogel eradicate biofilm and rescue stalled healing in chronic wounds, ACS Nano 13 (10) (2019) 11686–11697.

[6] Z. Cai, Y. Li, L. Bai, J. Xu, Z. Liu, T. Zhang, S. Gao, Y. Lin, Tetrahedral framework nucleic acids based small interfering RNA targeting receptor for advanced glycation end products for diabetic complications treatment, ACS Nano 17 (22) (2023) 22668–22683.

[7] J. Sun, W. Jia, H. Qi, J. Huo, X. Liao, Y. Xu, J. Wang, Z. Sun, Y. Liu, J. Liu, M. Zhen, C. Wang, C. Bai, An antioxidative and active shrinkage hydrogel integratedly promotes Re-epithelization and skin constriction for enhancing wound closure, Adv Mater 36 (21) (2024) e2312440.

[8] R. Fan, J. Zhao, L. Yi, J. Yuan, A. McCarthy, B. Li, G. Yang, J.V. John, W. Wan, Y. Zhang, S. Chen, Anti-inflammatory peptide-conjugated silk fibroin/cryogel hybrid dual fiber scaffold with hierarchical structure promotes healing of chronic wounds, Adv Mater 36 (16) (2024) e2307328.

[9] X. Qi, Y. Xiang, Y. Li, J. Wang, Y. Chen, Y. Lan, J. Liu, J. Shen, An ATP-activated spatiotemporally controlled hydrogel prodrug system for treating multidrug-resistant bacteria-infected pressure ulcers, Bioact. Mater. 45 (2025) 301–321.

[10] C. Tu, H. Lu, T. Zhou, W. Zhang, L. Deng, W. Cao, Z. Yang, Z. Wang, X. Wu, J. Ding, F. Xu, C. Gao, Promoting the healing of infected diabetic wound by an anti-bacterial and nano-enzyme-containing hydrogel with inflammation-suppressing, ROS-scavenging, oxygen and nitric oxide-generating properties, Biomaterials 286 (2022) 121597.

[11] Xiaoliang Qi, XinXin Ge, Xiaojing Chen, Erya Cai, Yajing Xiang, Hangbin Xu, Ying Li, Yulong Lan, Yizuo Shi, Hui Deng, Jianliang Shen, An immunoregulation hydrogel with controlled hyperthermia-augmented oxygenation and ROS scavenging for treating diabetic foot ulcers, Adv. Funct. Mater. 34 (33) (2024) 2400489.

[12] Y. Xiang, Z. Pan, X. Qi, X. Ge, J. Xiang, H. Xu, E. Cai, Y. Lan, X. Chen, Y. Li, Y. Shi, J. Shen, J. Liu, A cuttlefish ink nanoparticle-reinforced biopolymer hydrogel with robust adhesive and immunomodulatory features for treating oral ulcers in diabetes, Bioact. Mater. 39 (2024) 562–581.

[13] Y. Liu, G. Xia, Y. Chen, H. Xia, J. Xu, L. Guo, S. Lin, Y. Liu, Purpurolide C-based microneedle promotes macrophage-mediated diabetic wound healing via inhibiting TLR4-MD2 dimerization and MYD88 phosphorylation, Acta Pharm. Sin. B 13 (12) (2023) 5060–5073.
[14] Y. Xiong, Z. Lin, P. Bu, T. Yu, Y. Endo, W. Zhou, Y. Sun, F. Cao, G. Dai, Y. Hu, L. Lu, L. Chen, P. Cheng, K. Zha, M.A. Shahbazi, Q. Feng, B. Mi, G. Liu, A whole-course-repair system based on neurogenesis-angiogenesis crosstalk and macrophage reprogramming promotes diabetic wound healing, Adv Mater 35 (19) (2023) e2212300.
[15] Z. Li, B. Yang, Z. Yang, X. Xie, Z. Guo, J. Zhao, R. Wang, H. Fu, P. Zhao, X. Zhao, G. Chen, G. Li, F. Wei, L. Bian, Supramolecular hydrogel with ultra-rapid cell-mediated network adaptation for enhancing cellular metabolic energetics and tissue regeneration, Adv Mater 36 (15) (2024) e2307176.
[16] Z. Zhou, T. Deng, M. Tao, L. Lin, L. Sun, X. Song, D. Gao, J. Li, Z. Wang, X. Wang, J. Li, Z. Jiang, L. Luo, L. Yang, M. Wu, Snail-inspired AFG/GelMA hydrogel accelerates diabetic wound healing via inflammatory cytokines suppression and macrophage polarization, Biomaterials 299 (2023) 122141.
[17] C.O. Audu, S.J. Wolf, A.D. Joshi, J.Y. Moon, W.J. Melvin, S.B. Sharma, F.M. Davis, A.T. Obi, R. Wasikowski, L.C. Tsoi, E.C. Barrett, K.D. Mangum, T.M. Bauer, S. L. Kunkel, B.B. Moore, K.A. Gallagher, Histone demethylase JARID1C/KDM5C regulates Th17 cells by increasing IL-6 expression in diabetic plasmacytoid dendritic cells, JCI Insight 9 (12) (2024).
[18] K. Sun, Y.Y. Li, J. Jin, A double-edged sword of immuno-microenvironment in cardiac homeostasis and injury repair, Signal Transduct Target Ther 6 (1) (2021) 79.
[19] J. Luan, C. Truong, A. Vuchkovska, W. Guo, J. Good, B. Liu, A. Gang, N. Infarinato, K. Stewart, L. Polak, H.A. Pasolli, E. Andretta, A.Y. Rudensky, E. Fuchs, Y. Miao, CD80 on skin stem cells promotes local expansion of regulatory T cells upon injury to orchestrate repair within an inflammatory environment, Immunity 57 (5) (2024) 1071–1086.e7.
[20] D. Rütsche, M. Nanni, P. Cheng, N. Caflisch, A. Tastanova, C. Jenni, M.P. Levesque, U. Moehrlen, A.S. Klar, T. Biedermann, Human dermal microvascular arterial and venous blood endothelial cells and their use in bioengineered dermo-epidermal skin substitutes, Small Methods (2025) e2401588.
[21] S. He, Z. Li, L. Wang, N. Yao, H. Wen, H. Yuan, J. Zhang, Z. Li, C. Shen, A nanoenzyme-modified hydrogel targets macrophage reprogramming-angiogenesis crosstalk to boost diabetic wound repair, Bioact. Mater. 35 (2024) 17–30.
[22] X. Zhu, Y. Wang, I. Soaita, H.W. Lee, H. Bae, N. Boutagy, A. Bostwick, R.M. Zhang, C. Bowman, Y. Xu, S. Trefely, Y. Chen, L. Qin, W. Sessa, G. Tellides, C. Jang, N. W. Snyder, L. Yu, Z. Arany, M. Simons, Acetate controls endothelial-to-mesenchymal transition, Cell Metab. 35 (7) (2023) 1163–1178.e10.
[23] Y. Guo, S. Ding, C. Shang, C. Zhang, M. Li, Q. Zhang, L. Gu, B.C. Heng, S. Zhang, F. Mei, Y. Huang, X. Zhang, M. Xu, J. Jiang, S. Guo, X. Deng, L. Chen, Multifunctional PtCuTe nanosheets with strong ROS scavenging and ROS-independent antibacterial properties promote diabetic wound healing, Adv Mater 36 (8) (2024) e2306292.
[24] T. Liu, B. Xiao, F. Xiang, J. Tan, Z. Chen, X. Zhang, C. Wu, Z. Mao, G. Luo, X. Chen, J. Deng, Ultrasmall copper-based nanoparticles for reactive oxygen species scavenging and alleviation of inflammation related diseases, Nat. Commun. 11 (1) (2020) 2788.
[25] W. Liu, Y. Li, Y. Wang, Y. Feng, Bioactive metal-organic frameworks as a distinctive platform to diagnosis and treat vascular diseases, Small 20 (27) (2024) e2310249.
[26] Q. Liu, A. Zhang, R. Wang, Q. Zhang, D. Cui, A review on metal- and metal oxide-based nanozymes: properties, mechanisms, and applications, Nano-Micro Lett. 13 (1) (2021) 154.
[27] Y. Li, P. Li, Y. Chen, Y. Wu, J. Wei, Interfacial deposition of Ag nanozyme on metal-polyphenol nanosphere for SERS detection of cellular glutathione, Biosens. Bioelectron. 228 (2023) 115200.
[28] X. He, K. Gopinath, G. Sathishkumar, L. Guo, K. Zhang, Z. Lu, C. Li, E.T. Kang, L. Xu, UV-assisted deposition of antibacterial Ag-tannic acid nanocomposite coating, ACS Appl. Mater. Interfaces 13 (17) (2021) 20708–20717.
[29] Y. Li, Y. Wang, Y. Ding, X. Fan, L. Ye, Q. Pan, B. Zhang, P. Li, K. Luo, B. Hu, B. He, Y. Pu, A double network composite hydrogel with self-regulating Cu(2+)/luteolin release and mechanical modulation for enhanced wound healing, ACS Nano 18 (26) (2024) 17251–17266.
[30] Peizhe Li, Qiaoling Liu, Mengyu Pei, Yuci Gan, Yan Gong, Chuchen Gong, Pei Wang, Mingsong Wang, Xiansong Wang, Da-Peng Yang, Bo Liang, Guangyu Ji, Chlorogenic acid supported strontium polyphenol networks ensemble microneedle patch to promote diabetic wound healing, Chin. Chem. Lett. 35 (8) (2024).
[31] F. Huang, X. Lu, L. Kuai, Y. Ru, J. Jiang, J. Song, S. Chen, L. Mao, Y. Li, B. Li, H. Dong, J. Shi, Dual-site biomimetic Cu/Zn-mof for atopic dermatitis catalytic Therapy via suppressing FcγR-mediated phagocytosis, J. Am. Chem. Soc. 146 (5) (2024) 3186–3199.
[32] Y. Higashimura, T. Takagi, Y. Naito, K. Uchiyama, K. Mizushima, M. Tanaka, M. Hamaguchi, Y. Itoh, Zinc deficiency activates the IL-23/Th17 Axis to aggravate experimental colitis in mice, J Crohns Colitis 14 (6) (2020) 856–866.
[33] J. Zheng, T. Chen, K. Wang, C. Peng, M. Zhao, Q. Xie, B. Li, H. Lin, Z. Zhao, Z. Ji, B. Z. Tang, Y. Liao, Engineered multifunctional zinc-organic framework-based aggregation-induced emission nanozyme for accelerating spinal cord injury recovery, ACS Nano 18 (3) (2024) 2355–2369.
[34] F. Yang, Y. Xue, F. Wang, D. Guo, Y. He, X. Zhao, F. Yan, Y. Xu, D. Xia, Y. Liu, Sustained release of magnesium and zinc ions synergistically accelerates wound healing, Bioact. Mater. 26 (2023) 88–101.
[35] H. Long, Z. Xin, F. Zhang, Z. Zhai, X. Ni, J. Chen, K. Yang, P. Liao, L. Zhang, Z. Xiao, D. Sindaye, B. Deng, The cytoprotective effects of dihydromyricetin and associated metabolic pathway changes on deoxynivalenol treated IPEC-J2 cells, Food Chem. 338 (2021) 128116.
[36] D. Liu, Y. Mao, L. Ding, X.A. Zeng, Dihydromyricetin: a review on identification and quantification methods, biological activities, chemical stability, metabolism and approaches to enhance its bioavailability, Trends Food Sci. Technol. 91 (2019) 586–597.
[37] J. Yang, L. Zhang, Y. Wang, N. Wang, H. Wei, S. Zhang, Q. Ding, S. Sun, C. Ding, W. Liu, Dihydromyricetin-loaded oxidized polysaccharide/L-arginine chitosan adhesive hydrogel promotes bone regeneration by regulating PI3K/AKT signaling pathway and MAPK signaling pathway, Carbohydr. Polym. 346 (2024) 122614.
[38] X. Qi, E. Cai, Y. Xiang, C. Zhang, X. Ge, J. Wang, Y. Lan, H. Xu, R. Hu, J. Shen, An immunomodulatory hydrogel by hyperthermia-assisted self-cascade glucose depletion and ROS scavenging for diabetic foot ulcer wound therapeutics, Adv Mater 35 (48) (2023) e2306632.
[39] X. Liang, H. Chen, R. Zhang, Z. Xu, G. Zhang, C. Xu, Y. Li, L. Zhang, F.J. Xu, Herbal micelles-loaded ROS-responsive hydrogel with immunomodulation and microenvironment reconstruction for diabetic wound healing, Biomaterials 317 (2025) 123076.
[40] Q. Li, M. Dong, Q. Han, Y. Zhang, D. Yang, D. Wei, Y. Yang, Enhancing diabetic wound healing with a pH-responsive nanozyme hydrogel featuring multi-enzyme-like activities and oxygen self-supply, J Control Release 365 (2024) 905–918.
[41] Y. Qian, Y. Zheng, J. Jin, X. Wu, K. Xu, M. Dai, Q. Niu, H. Zheng, X. He, J. Shen, Immunoregulation in diabetic wound repair with a photoenhanced glycyrrhizic acid hydrogel scaffold, Adv Mater 34 (29) (2022) e2200521.
[42] W. Zhang, K. Zha, Y. Xiong, W. Hu, L. Chen, Z. Lin, C. Yu, W. Zhou, F. Cao, H. Hu, B. Mi, G. Liu, Glucose-responsive, antioxidative HA-PBA-FA/EN106 hydrogel enhanced diabetic wound healing through modulation of FEM1b-FNIP1 axis and promoting angiogenesis, Bioact. Mater. 30 (2023) 29–45.
[43] J. Huang, R. Yang, J. Jiao, Z. Li, P. Wang, Y. Liu, S. Li, C. Chen, Z. Li, G. Qu, K. Chen, X. Wu, B. Chi, J. Ren, A click chemistry-mediated all-peptide cell printing hydrogel platform for diabetic wound healing, Nat. Commun. 14 (1) (2023) 7856.
[44] V. Kloubert, L. Rink, Zinc as a micronutrient and its preventive role of oxidative damage in cells, Food Funct. 6 (10) (2015) 3195–3204.
[45] A. Mendoza, P. Patel, D. Robichaux, D. Ramirez, J. Karch, Inhibition of the mPTP and lipid peroxidation is additively protective against I/R injury, Circ. Res. 134 (10) (2024) 1292–1305.
[46] K. De Bock, M. Georgiadou, S. Schoors, A. Kuchnio, B.W. Wong, A.R. Cantelmo, A. Quaegebeur, B. Ghesquière, S. Cauwenberghs, G. Eelen, L.K. Phng, I. Betz, B. Tembuyser, K. Brepoels, J. Welti, I. Geudens, I. Segura, B. Cruys, F. Bifari, I. Decimo, R. Blanco, S. Wyns, J. Vangindertael, S. Rocha, R.T. Collins, S. Munck, D. Daelemans, H. Imamura, R. Devlieger, M. Rider, P.P. Van Veldhoven, F. Schuit, R. Bartrons, J. Hofkens, P. Fraisl, S. Telang, R.J. Deberardinis, L. Schoonjans, S. Vinckier, J. Chesney, H. Gerhardt, M. Dewerchin, P. Carmeliet, Role of PFKFB3-driven glycolysis in vessel sprouting, Cell 154 (3) (2013) 651–663.
[47] C. Song, S. Wang, Z. Fu, K. Chi, X. Geng, C. Liu, G. Cai, X. Chen, D. Wu, Q. Hong, IGFBP5 promotes diabetic kidney disease progression by enhancing PFKFB3-mediated endothelial glycolysis, Cell Death Dis. 13 (4) (2022) 340.
[48] F. Xie, B. Liu, W. Qiao, J.Z. He, J. Cheng, Z.Y. Wang, Y.M. Hou, X. Zhang, B.H. Xu, Y. Zhang, Y.G. Chen, M.X. Zhang, Smooth muscle NF90 deficiency ameliorates diabetic atherosclerotic calcification in male mice via FBXW7-AGER1-AGEs axis, Nat. Commun. 15 (1) (2024) 4985.
[49] Y. Yuan, G. Fan, Y. Liu, L. Liu, T. Zhang, P. Liu, Q. Tu, X. Zhang, S. Luo, L. Yao, F. Chen, J. Li, The transcription factor KLF14 regulates macrophage glycolysis and immune function by inhibiting HK2 in sepsis, Cell. Mol. Immunol. 19 (4) (2022) 504–515.
[50] S. Wang, Y. Liu, X. Wang, L. Chen, W. Huang, T. Xiong, N. Wang, J. Guo, Z. Gao, M. Jin, Modulating macrophage phenotype for accelerated wound healing with chlorogenic acid-loaded nanocomposite hydrogel, J Control Release 369 (2024) 420–443.
[51] C.O. Audu, W.J. Melvin, A.D. Joshi, S.J. Wolf, J.Y. Moon, F.M. Davis, E.C. Barrett, K.D. Mangum, H. Deng, X. Xing, R. Wasikowski, L.C. Tsoi, S.B. Sharma, T.M. Bauer, J. Shadiow, M.A. Corriere, A.T. Obi, S.L. Kunkel, B. Levi, B.B. Moore, J. E. Gudjonsson, A.M. Smith, K.A. Gallagher, Macrophage-specific inhibition of the histone demethylase JMJD3 decreases STING and pathologic inflammation in diabetic wound repair, Cell. Mol. Immunol. 19 (11) (2022) 1251–1262.
[52] P. Cheng, X. Xie, L. Hu, W. Zhou, B. Mi, Y. Xiong, H. Xue, K. Zhang, Y. Zhang, Y. Hu, L. Chen, K. Zha, B. Lv, Z. Lin, C. Lin, G. Dai, Y. Hu, T. Yu, H. Hu, G. Liu, Y. Zhang, Hypoxia endothelial cells-derived exosomes facilitate diabetic wound healing through improving endothelial cell function and promoting M2 macrophages polarization, Bioact. Mater. 33 (2024) 157–173.
[53] L.F. Loffredo, T.M. Savage, O.R. Ringham, N. Arpaia, Treg-tissue cell interactions in repair and regeneration, J. Exp. Med. 221 (6) (2024).
[54] S. Knoedler, L. Knoedler, M. Kauke-Navarro, Y. Rinkevich, G. Hundeshagen, L. Harhaus, U. Kneser, B. Pomahac, D.P. Orgill, A.C. Panayi, Regulatory T cells in skin regeneration and wound healing, Mil Med Res 10 (1) (2023) 49.
[55] T. Wei, T. Pan, X. Peng, M. Zhang, R. Guo, Y. Guo, X. Mei, Y. Zhang, J. Qi, F. Dong, M. Han, F. Kong, L. Zou, D. Li, D. Zhi, W. Wu, D. Kong, S. Zhang, C. Zhang, Janus liposozyme for the modulation of redox and immune homeostasis in infected diabetic wounds, Nat. Nanotechnol. 19 (8) (2024) 1178–1189.
[56] W. Zhou, Z. Duan, J. Zhao, R. Fu, C. Zhu, D. Fan, Glucose and MMP-9 dual-responsive hydrogel with temperature sensitive self-adaptive shape and controlled drug release accelerates diabetic wound healing, Bioact. Mater. 17 (2022) 1–17.

[57] W. Zhang, Z. Ge, Y. Xiao, D. Liu, J. Du, Antioxidant and immunomodulatory polymer vesicles for effective diabetic wound treatment through ROS scavenging and immune modulating, Nano Lett. 24 (31) (2024) 9494–9504.
[58] L. Kulik, M. Maywald, V. Kloubert, I. Wessels, L. Rink, Zinc deficiency drives Th17 polarization and promotes loss of Treg cell function, J. Nutr. Biochem. 63 (2019) 11–18.
[59] H. Jing, Y. Ren, Y. Zhou, M. Xu, S. Krizkova, Z. Heger, Q. Lu, S. Wang, X. Liang, V. Adam, N. Li, Remodeling of the liver fibrosis microenvironment based on nilotinib-loaded multicatalytic nanozymes with boosted antifibrogenic activity, Acta Pharm. Sin. B 13 (12) (2023) 5030–5047.